ARTICLE IN PRESS

CHEMGE-17857; No of Pages 18

Chemical Geology xxx (2016) xxx-xxx



Contents lists available at ScienceDirect

Chemical Geology

journal homepage: www.elsevier.com/locate/chemgeo



Measuring silicate mineral dissolution rates using Si isotope doping

Chen Zhu ^{a,*}, Zhaoyun Liu ^{a,b}, Yilun Zhang ^c, Chao Wang ^a, Augustus Scheafer ^a, Peng Lu ^{a,1}, Guanru Zhang ^a, R. Bastian Georg ^d, Hong-lin Yuan ^e, J. Donald Rimstidt ^f

- ^a Department of Geological Science, Indiana University, Bloomington, IN 47405, USA
- ^b School of Earth Sciences, Zhejiang University, Hangzhou 300027, People's Republic of China
- ^c Doctoral Program in Environmental Science, Indiana University, Bloomington, IN 47405, USA
- ^d Water Research Center, Trent University, Peterborough, ON, Canada
- ^e Northwest University, Department of Geology, State Key Laboratory Continental Dynamic, Xi'an 710069, People's Republic of China
- f Department of Geological Sciences, Virginia Tech, Blacksburg, VA 24061, USA

ARTICLE INFO

Article history: Received 14 October 2015 Received in revised form 15 February 2016 Accepted 27 February 2016 Available online xxxx

Keywords: Kinetics Feldspar Si isotope Reaction rates

ABSTRACT

New experimental data and quantitative models show that the ²⁹Si doping experimental technique (Gruber, Zhu, and others, 2013, GCA) is robust for measuring silicate mineral dissolution rates even while a Si-containing secondary phase is precipitating. In this study, batch experiments of albite dissolution were conducted under ambient temperature and pH 3-7.5, some seeded with kaolinite. Initial solutions of various Si concentrations were doped with ²⁹Si, resulting in a Si isotopic composition highly anomalous to natural Si isotope compositions. The isotopic contrast and precision of isotope fraction analysis to ± 0.0005 to ± 0.001 allow detection of the dissolution of a minuscule amount of albite in aqueous solutions. Experimental data and quantitative modeling show Si isotope fractionation during albite dissolution ranged from $^{30}\epsilon_{sol-ab}-2.870$ to 0.804%, significant for Si biogeochemical cycling, but resulting in only <\\pm 0.04\% errors in rate determination. The simultaneous precipitation of secondary phases consumed silica, causing slight changes of Si isotope ratios, but the isotopic fractionation due to secondary phase precipitation is negligible for determining albite dissolution rates. Combination of Si isotopes and Si concentrations, precisely measured with the Si isotope dilution method, allowed determination of secondary phase precipitation rates simultaneously. This means that we can now measure rates at circumneutral pH and near equilibrium conditions, even when secondary precipitates are forming. However, while the isotope doping method has greatly improved the precision and sensitivity of rate measurements, the accuracy of rate measurements is still subject to the vagaries of sample preparation and other unknown effects as shown our data near pH 5.5. When the solution is very close to equilibrium, the backward reaction becomes important and interpretation of the isotope data would be complicated or impossible.

 $\ensuremath{\mathbb{C}}$ 2016 Elsevier B.V. All rights reserved.

1. Introduction

The isotopic doping technique used in the present paper introduces an enriched rare isotope of a given element to an experimental solution interacting with a mineral or a suite of minerals that have normal or natural isotopic compositions (Beck et al., 1992; Gaillardet, 2008). Monitoring the isotopic compositions of the solution allows mineral dissolution rates to be determined with the help of the extreme sensitivity of modern mass spectrometer measurements. Because the precipitation of the isotope into secondary phases does not significantly change the isotopic ratios of the fluids, dissolution rates can be measured even when secondary phase precipitation occurs. Therefore, the method allows measurements of

* Corresponding author.

reaction kinetics near equilibrium. This method has been successfully applied using ³⁹K and ⁸⁴Sr simultaneously to measure rates of dissolution of K-feldspar, biotite, and plagioclase during the hydrothermal alteration of a granite in conditions close to equilibrium (Zuddas et al., 1995; Seimbille et al., 1998). Also, ⁸⁴Sr/⁸⁷Sr and ⁴⁴Ca/⁴²Ca doping was used to measure rates of calcite recrystallization and conversion from aragonite to calcite (Beck et al., 1992; Berndt and Seyfried, 1999). Finally, ²⁹Si and ³⁰Si were used to find albite dissolution rates (Gruber et al., 2013; Gruber et al., 2014; Zhu et al., 2014).

Although Si isotopes have been measured for over 50 years, the recent advances in high resolution MC-ICP-MS now allow Si isotopes to be analyzed relatively quickly, with minimal sample preparation and with a higher precision (Georg et al., 2006). The main advantage of using Si stable isotopes is that they are part of the silicate mineral structure. Here, we have utilized stable Si isotopes as a way to overcome the sensitivity issues by using "Si isotope spikes" in the initial solution in the batch reactor and by using isotope dilution method to measure the Si

http://dx.doi.org/10.1016/j.chemgeo.2016.02.027 0009-2541/© 2016 Elsevier B.V. All rights reserved.

E-mail address: chenzhu@indiana.edu (C. Zhu).

Now at EXPEC Advance Research Center, Saudi Aramco Oil Company, Dhahran 31311, Saudi Arabia.

concentrations with much smaller errors than the conventional chemical analysis.

Feldspars comprise over 50% of the volume of the earth's crust. Establishing reliable rates for low-temperature feldspar dissolution is essential to quantify many fundamental geological and environmental processes. Among these are the functional relationship between silicate weathering and the global climate over geologic time (Berner and Berner, 1997), controls on surface and groundwater quality, global elemental cycling (Lasaga et al., 1994), the availability of inorganic nutrients in soils (Federer et al., 1989; Likens et al., 1998), impacts of acid mine drainage, neutralization of acid precipitation in watersheds (Drever and Clow, 1995), safety of nuclear waste repositories (Spycher et al., 2003), and geological carbon sequestration (White et al., 2003).

One outstanding problem of great significance in modern geochemistry is the apparent discrepancy between laboratory-measured and field derived feldspar dissolution rates (Velbel, 1990; Brantley, 1992; Blum and Stillings, 1995; Drever and Clow, 1995; Zhu, 2005). This discrepancy is significant, up to 2 to 5 orders of magnitude, and can lead to dramatically different modeling results. Obviously, there are several ways to frame this apparent discrepancy, as conditions under which feldspar dissolves in field and laboratory are surely different and we must take pains to ensure comparing equivalent processes and conditions. However, the resolution of this apparent discrepancy is hampered by the experimental challenges at ambient temperatures. Silicate reactions at room temperature are slow for experiments near neutral pH where most reactions occur in nature. In addition, at near equilibrium conditions, the experimental solutions are often supersaturated with secondary phases. Their precipitation depletes Si from solution, causing an apparent lower dissolution rate. New experimental techniques are needed to overcome these obstacles and resolve the apparent discrepancy.

In this paper we first present new experimental data on Si isotope doping and isotopic fractionation during albite dissolution. Then we evaluate possible interferences on determining the rates, namely (A) isotopic fractionation during albite dissolution, (B) precipitation of a Si-containing secondary phase, and (C) Si isotope fractionation during the precipitation of the secondary phase. Three conceptual models were developed, progressively including above three interferences (termed Model A, B, C), and these models were applied to the experimental data. Our results show that all three interferences have negligible effects on determination of albite dissolution rates, which makes this new experimental method particularly useful for measuring albite dissolution rates while a Si-containing secondary phase is precipitating. We further demonstrate that, together with silicon concentration data—particularly the more precise silicon concentration data from the isotope dilution method, the rate of secondary phase precipitation can also be determined from the isotope data. Finally, based on our experimental data and the above conceptual models, we predicted optimal experimental conditions for measuring silicate mineral dissolution over a wide range of rates.

2. Materials and methods

Part of the isotope doping methodology described below was described in earlier publications (Gruber et al., 2013; Lu et al., 2013). For completeness, we repeat some essential details.

2.1. Albite grains preparation

Research grade albite crystals (from Amelia Court House, Virginia, USA and from Evje, Norway) were purchased from the Ward's Natural Science Establishment, Inc. The crystals were handpicked, ground with a clean agate mortar and pestle, and subsequently dry sieved through clean copper mesh to retain the $53{\text -}106~\mu{\rm m}$ fraction. For the freshly ground material, there were a large number of submicron-to-micron

particles that adhered to the surface of large grains. Dissolution of these ultra-fine particles will result in initially non-linear rates of reaction or parabolic kinetics (Holdren and Berner, 1979; Lu et al., 2013). To remove these particles, the ground feldspar sample was ultrasonically rinsed with ethanol eight times for about 20 min per treatment. The cleaned feldspar grains were then rinsed with deionized (DI) water and freeze-dried. They were examined under SEM to observe the particle morphology, size distribution, and cleaned surface (Fig. 1a). Finally, the cleaned feldspar samples were kept in an oven at 100 °C overnight to exclude all possible organic contamination and were then stored in a desiccator. See below (Section 2.7) for X-ray diffraction analysis of the samples.

2.2. Kaolinite pre-treatment

Florida kaolinite from Ward's Natural Science Establishment, Inc. and a sample of Georgia kaolinite were filtered through a 38 µm sieve using deionized water to eliminate any possible coarse grained contaminants. The remaining mixtures were then dried in an oven over night at 100 °C. They were then mounted in separate titanium 1.5 cm front pack mounts for X-ray diffraction to determine the purity of the sample. The analysis revealed the Florida sample to be 88.12% kaolinite and 11.88% dickite and the Georgia sample to be 82.97% kaolinite and 17.03% dickite. Based on these results the Florida kaolinite was used in the experiments.

The treatment of the Florida kaolinite sample in this study followed the method described in Yang and Steefel (2008). The sample was first cleaned in order to remove amorphous oxy-hydroxide material before

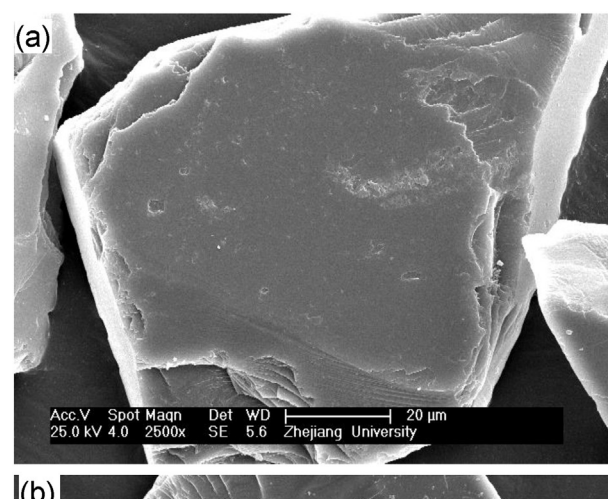




Fig. 1. FEI-SEM micrographs of albite grains pre (a) and after (b) after 60 day's reaction in pH \sim 5 solutions.

being used as seed material in the dissolution experiments. The sample was put into a 50 mL centrifuge tube and topped off with 1 M NaCl at pH 3. That tube was then inserted in an ultrasonic bath for 10 min before being removed and inserted in the centrifuge for 5 min. After centrifugation, the supernatant was pipetted off and the rinsing process was repeated until the supernatant reached pH 3. The ultrasonication/centrifugation process was then performed with deionized water in order to rinse away the NaCl. This was repeated until the supernatant pH was greater than 5. The remaining sample was then put on a vacuum filter to facilitate the drying process before being dried in an oven overnight at 50 °C and stored in a desiccator.

2.3. Dissolution experiments without isotope doping

Except where noted, all chemicals used are analytical grade. 99.00 g DI water (18.2 M Ω , Millipore) and 1.00 mL 1.00 M KCl stock solution was added into each wide-mouth polypropylene bottle (4 oz and 125 mL, Fisher Scientific, Pittsburgh, PA, USA). The solution pH was thereafter measured and adjusted by adding a small amount (<0.10 mL) of 1.0 N HCl, 0.10 N HCl, 0.01 N HCl, 0.10 N KOH, and/or 0.01 N KOH to a final value of 3.00 (\pm 0.05), 5.00 (\pm 0.05), or 7.00 (± 0.05) . Additionally, 0.250 (± 0.001) g of mineral sample was added into each bottle to initiate the mineral dissolution. The bottles were sealed with parafilm in order to limit the potential diffusion of CO₂ into the bottle headspace, which would result in CO₂ dissolution and pH decrease. The bottles were agitated at ~22.0 (± 0.5) °C on an orbital shaker (VRN-200, Gemmy Industrial Corporation, Taipei, Taiwan, China; or Model 2345Q, Thermo Scientific) at ~100 rpm. At the pre-determined sampling interval, bottle solution was poured into a vacuum filter system to separate the solids from the solution. The experimental solutions had only dilute Si elemental concentrations so that solutions were concentrated by evaporation to reduce the solution volume by five times.

2.4. Dissolution experiments with isotope doping

Isotope stock solution (1.6 mM ²⁹SiO₂) was prepared by dissolving 0.0293 g ²⁹Si-enriched SiO₂ powder (0.0004 ²⁸Si, 0.9990 ²⁹Si, and 0.0006 ³⁰Si from Isoflex, San Francisco, CA, USA) with 300 mL 33,3% KOH solution (150 g KOH dissolved in 300 g DI water) for about one week and was then stored in a refrigerator at 4.0 °C. The ²⁹Si concentration in experimental solution was controlled to 40 µM by adding 2.50 mL 1.6 mM ²⁹SiO₂ stock solution, 95.65 g (equivalently 95.68 mL) DI water, 1.22 mL 37% (12.1 N) HCl solution, and 0.600 mL 3 N HCl solution into each wide-mouth polypropylene bottle (4 oz and 125 mL, Fisher Scientific, Pittsburgh, PA, USA) with the final solution volume close to ~100 mL. The solution pH was thereafter measured and adjusted by adding small amount (<0.50 mL) of 1.0 N HCl or 1.0 N KOH to a final value of 3.00 (\pm 0.05), 5.00 (\pm 0.05), or 7.00 (\pm 0.05). Additionally, $0.250~(\pm\,0.001)~g$ of albite was added into each bottle to initiate the mineral dissolution. For experiments with kaolinite seeds, 0.001 g kaolinite was added. The polypropylene bottles were sealed with parafilm and were agitated at room temperature of 22.5 (± 0.5) °C on an orbital shaker (VRN-200, Gemmy Industrial Corporation, Taipei, Taiwan, China) at ~100 rpm.

2.5. Sampling of dissolution experiments

At the pre-determined sampling interval, the solution pH was quickly measured. Then, the solution was poured into a vacuum filter system (Thermo Scientific, Nalgene, sterile analytical filter) which used a piece of 0.22 µm nitrocellulose membrane filter paper (Fisher Scientific, Pittsburgh, PA, USA) to separate the solids from the 89.5 g solution. The filtered solution was weighted and mixed with 0.500 mL (equivalently 0.50 g) of 5% HCl solution in a polypropylene wide-mouth bottle (4 oz and 125 mL, Fisher Scientific, Pittsburgh, PA, USA) in order to make the solution unsaturated with respect to its secondary phases (such as

kaolinite and gibbsite). The solids on the filter paper were thereafter rinsed with several mL DI water for five times to wash off residual solution, transferred into a plastic container with a spoon, air-dried overnight, and then stored in a desiccator. These solid samples were selected for examination under SEM and XRD.

2.6. Sample pre-treatment before isotopic analysis

In order to reduce high concentrations of cations that might interfere with the silicon isotope analysis, all solution samples were pretreated with cation exchange resin (AG 50W-X8, Bio-Rad Laboratories, Inc., Hercules, CA, USA) before Si isotope analysis, following the method of Georg et al. (Georg et al., 2006). Briefly, 1.8 mL of the cation exchange resin (resin on column cleaning) was placed in a 10 mL Poly-Prep chromatography column (Bio-Rad Laboratories, Inc., Hercules, CA, USA) and was then rinsed with 6.0 mL DI water, 6.0 mL 3.0 N HCl, 6.0 mL 6.0 N HCl, 4.0 mL 37% HCl, 6.0 mL 6.0 N HCl, 10 mL 3.0 N HCl, and three times of 5.0 mL DI water. The treated resin in the column was then further rinsed with 1.00 mL of solution sample. Afterwards, 7.0 mL of the solution sample was loaded into the column and the filtered rated solution was collected in a clean polystyrene 15 mL conical centrifuge tube (Fisher Scientific, Pittsburgh, PA, USA).

2.7. Mineral characterization

Amelia albite it is a nearly pure end-member albite (e.g., see Harlow and Brown, 1980; Smith and Brown, 1988; Harouiya and Oelkers, 2004). The reported structure formula is $K_{0.009}Na_{0.974}Ca_{0.007}Al_{1.031}Si_{2.976}O_8$. The pegmatic Evje albite from Norway was analyzed with electron microprobe analysis by Knauss and Wolery (1986). The chemical composition is very pure albite (99%), with SiO₂ 68.59%, Al₂O₃ 20.30%, Na₂O 10.99%, K₂O 0.09%. Knauss and Wolery (1986) also carried out powder X-ray diffraction of the Evje albite and found it only slightly disordered. They suggested that Helgeson et al. (1978)'s "low albite" is suitable for thermodynamic calculations.

Our powder X-ray diffraction analyses were carried out using a Bruker D8 Advance diffractometer, equipped with a Cu anode at 20 kV and 5 mA, and with a SolX energy-dispersive detector. The scan parameters used were 2 to 70° 2 θ , with a step size of 0.02° 2 θ . Starting samples were ground by hand in an agate mortar and pestle to get sufficient small particles. These particles were subsequently filled into the cavity of a titanium sample holder for XRD analysis. Results confirm that the reported Evje albite contains 95.05% low-albite, 2.94% muscovite and 2.01% quartz.

A Beckman Coulter SA-3100 surface area analyzer was used for the Brunauer–Emmett–Teller (BET) (Braunauer et al., 1938) surface area analysis of albite grains before the experiments. The samples were degassed at 250 °C overnight prior to measurements. The instrument was calibrated before and during measurements periodically, using National Institute of Standards and Technology reference material 1900, a silicon nitrite powder with surface area of 2.85 m²/g. Multipoint N₂ gas adsorption isotherms were measured to obtain BET specific surface area of for albite (Lu et al., 2013). Multipoint N₂ gas adsorption isotherms were measured to obtain the specific surface area of Evje albite ~0.143 m²/g (\pm 5%) and of Amelia albite of 0.13 m²/g (\pm 5%).

Scanning Electron Microscopy (SEM) was conducted with a Quanta 400 Field Emission Gun (FEG). The Energy Dispersive X-ray Spectrometer (EDS) system has an EDAX thin window and CDU LEAP detector. The low energy X-ray detection with FEG provided high spatial resolution for microanalysis down to $\sim\!0.1~\mu\text{m}^2$ under optimum conditions.

2.8. Measurements of silicon stable isotopes

The Si isotope ratios and compositions were measured using high-resolution multiple-collector inductively coupled plasma mass spectrometry (HR-MC-ICP-MS) at Trent University. The analyses utilized

4

their recently upgraded Thermo Fisher Neptune *PLUS*. Blank samples were filled with ultrapure deionized water and were acidified with ultrapure HCl.

Naturally occurring silicon has three stable isotopes ²⁸Si (0.92229). 29 Si (0.04683) and 30 Si (0.03087), where the numbers in parenthesis represent their natural fractions, respectively. Isotope fractions in the experimental samples were determined by means of MC-ICP-MS. Silicon isotope analyses on MC-ICP-MS require high-mass resolving capabilities to resolve polyatomic species that interfere with the Si massspectrum, especially high abundances of N2 and NO species on masses ²⁸Si and ³⁰Si (Georg et al., 2006). The Thermo Fisher Neptune Plus MC-ICP-MS is capable of providing resolving power sufficient to resolve all polyatomic species that interfere with the Si mass-spectrum. Isotope analyses are typically performed in medium resolution with a resolving power of $m/\Delta m = 6000$. During mass-spectrometric analyses, all three Si isotope masses were measured simultaneous to overcome intrinsic noise associated with the plasma ion-source in order to ensure that isotope ratios are determined with a typical precision better than 0.1%. Instrumental mass discrimination was corrected by using an Mg isotope standard as an internal tracer. The certified Mg isotope standard DSM-3 was added to samples and standards and the three stable isotopes of Mg (24Mg, 25Mg and 26Mg) were analyzed simultaneously alongside the Si isotopes. The measured Mg ratios were then normalized to the certified values to provide a correction factor as a measure of instrumental discrimination, which was then applied to the measured Si isotope ratios. The rationale behind this correction method is that isotopes with similar masses experience similar levels of instrumental massdiscrimination. Samples (~0.5 ppm Si) were introduced into the plasma via a self-aspirating micro-concentric PFA nebulizer and an Apex desolvation device. Silicon backgrounds were corrected for by onpeak-zero measurements, where a blank solution (2% HNO₃) was analyzed instead of a sample. The blank intensities were then subtracted from the signals of the subsequent sample analyses. Typical signal intensities for an uptake rate of 0.1 mL/min were approximately 60 V for a solution containing 1 ppm Si.

The solid material was dissolved in a Si-free medium and samples were taken at a defined interval. Detailed experimental procedure is described in Georg et al. (2006). The measurement results show that the isotope fractions of ^{28}Si , ^{29}Si , and ^{30}Si in the Amelia albite are 0.9223, 0.0467, and 0.0310, respectively (See Table 1 for symbols). The isotope fractions of ^{28}Si , ^{29}Si , and ^{30}Si in the Evje albite are 0.9223, 0.0467, and 0.0311, respectively (Table 2).

Silicon isotope data are commonly reported as deviations of ${}^{30}Si/{}^{28}Si$ and ${}^{29}Si/{}^{28}Si$ from the international standard NBS-28 in parts per mil (with $R_{30/28} = {}^{30}Si/{}^{28}Si$ or $R_{29/28} = {}^{29}Si/{}^{28}Si$) as follows (Georg et al., 2009):

$$\delta^{x} \text{Si} = \left(\frac{R_{x/28,sample}}{R_{x/28,NRS-28}} - 1\right) \times 1000 \tag{1}$$

where x stands for 29 or 30. For the Amelia albite, these values are $\delta^{29}{\rm Si}=-0.110\%$ and $\delta^{30}{\rm Si}=-0.256\%$, respectively (see Table 1 for symbols).

2.9. Determination of elemental Si concentrations [SiO₂]

For the isotopically doped albite dissolution experiments (Section 2.4), if there is no isotopic fractionation during albite dissolution and the amount of secondary Si-containing mineral precipitation is negligible, the system is a two end-member mixture of albite and initial aqueous solution. The measured isotopic fractions in the experimental solutions should give us the aqueous concentrations [SiO₂] (termed IX method hereafter).

Table 1List of symbols and definitions

Symbols	Explanations
$[SiO_2]^t$	Total dissolved silicon concentration (μ M) in experimental solution sampled after time t from the start of the experiment
$[SiO_2]_{spi}$	Total dissolved silicon concentration (μM) in spike (stock) solution used for isotopic dilution analysis of [SiO ₂] _t
$[SiO_2]^{tO}$	Silicon concentration (μ M) in initial solution at $t=0$
[SiO ₂] _{mix}	Silicon concentration (μ M) in the mixed solution (experimental solution + spike, $V_1 + V_2$) for
²⁸ SiO ₂]	isotope dilution analysis 28 Si concentration (μ M), [28 SiO ₂] = [SiO ₂] t . 28 Si, similarly for 29 Si, 30 Si
$\eta_{28\mathrm{Si},j}$	Mole of 28Si in the jth mineral, similarly for $n_{29\text{Si},i}$ and $n_{30\text{Si},j}$
/ 1	Volumes (mL) of experimental solution used for isotope dilution
/2	Volumes (mL) of analytical spike solution used for isotope dilution
/	Volume of solution in dissolution experiments (~100 mL)
⁸ Si ^t	²⁸ Si fraction (0 to 1.0) in experimental solution sampled after time <i>t</i> ; similarly for ²⁹ Si ^t and ³⁰ Si ^t
²⁸ Si _{spi}	²⁸ Si fraction (0 to 1.0) in spike (stock) solution used for isotopic dilution analysis; similarly for ²⁹ Si _{spi} and ³⁰ Si _{spi}
²⁸ Si _{mix}	²⁸ Si fraction (0 to 1.0) in the mixed solution (experimental solution + spike) for isotope dilution analysis; similarly for ²⁹ Si _{mix} and ³⁰ Si _{mix}
²⁸ Si _{ab}	²⁸ Si fraction of albite crystals; similarly for $^{29}Si_{ab}$ and $^{30}Si_{ab}$
²⁸ Si ^{t0}	²⁸ Si fraction of initial solutions at $t = 0$; similarly for ²⁹ Si ^{t0} and ³⁰ Si ^{t0}
j	Rate of dissolution or precipitation of the <i>j</i> th mineral in mol m^{-2} s ⁻¹
- [/] j,28	Rate of dissolution or precipitation of the <i>j</i> th mineral regarding to 28 Si in mol L^{-1} s ⁻¹ ;
r'_j	similarly for other silicon isotopes Rate of dissolution or precipitation of the jth mineral in mol L ⁻¹ s ⁻¹ $r'_j = r \pmod{m^{-2} s^{-1}} \cdot S_{Aj} \pmod{r^2} L$
Δt	Time Time to time $t + 1$
^y ab	Stoichiometric coefficient of Si in
^U kao	molecular formula of albite Stoichiometric coefficient of Si in
	secondary mineral precipitate
R_i $\Delta G_{r,i}$	Isotope ratio in phase A Gibbs free energy of reaction for
•	the jth mineral (J/mol)
ζ	Equilibrium constant Reactive surface area of the jth mineral (m ² /L)
o _{Aij} Si _A	The δ -notation of silicon isotope composition in phase A (%): $\delta^{30} Si_A = (\frac{R_A}{R_{NBS-2B}} - 1) \times 1000$
Δ^{30} Si _{A-B}	similarly for δ^{29} Si _A The difference in δ^{30} Si value between phases A and B (%): Δ^{30} Si _{A-B} = δ^{30} Si _A - δ^{30} Si _B
χ_{A-B}	Similarly for $\Delta^{29} \mathrm{Si}_{A-B}$ Fractionation factor α between phases A and B
$^{30}\epsilon_{A-B}$	$\alpha_{A-B} = R_A/R_B$ Enrichment factor ε between phases A and B ; similarly for $^{29}\varepsilon_{A-B}$
$lpha'{}_{ab}$	30 $\varepsilon_{i-j} = 1000 \times \ln \alpha_{A-B}$ Kinetic fractionation factor (α') in the dissolution process
	$lpha_{ab}' = rac{1}{R_{ab}} I_{ab,30}' igg/_{r_{ab,28}'}$
α'_{kao}	Kinetic fractionation factor (α') in the precipitation process

Table 1 (continued)

Symbols	Explanations			
	$lpha_{kao}' = rac{1}{R_{sol}} r_{kao.30}' \Big/_{r_{kao.28}'}$			
\mathcal{E}'_{ab}	Kinetic fractionation factor (ε') in the dissolution process; similarly for ε'_{kao} $\varepsilon_{ab'} = 1000 \ln \alpha_{ab'}$			
$K_{x,kao}$	$\varepsilon_{ab} = 1000 \mathrm{m} \alpha_{ab}$ Fractionation modifier			
λ,καο	$r'_{xkao} = \kappa_{x,kao}{}^{x} Si_{sol} r'_{kao}$			
	Similarly for $\kappa_{x,ab}$			
f	Fraction of Si that remains in the			
•	$solution f = [SiO_2]^t / [SiO_2]^{t0}$			
Abbrev				
spi	Spike			
dis	Dissolution			
ab	Albite			
pre	Precipitate			
kao	Kaolinite			
gbs	Gibbsite			
aq	Aqueous species			
qtz	Quartz			
fsp	Feldspar			
sol	Solution			
DSi	Dissolved silica			
S-T	Short-term			
L-T	Long-term			
IX	Isotope mixing method			
ID	Isotope dilution method			

From mass balance consideration for each of the Si isotopes we calculated the $[SiO_2]$ from the following equation

$$[\mathrm{SiO}_2]^t = \left(\frac{^{28}\mathrm{S}i^{t0} - ^{28}\mathrm{S}i_{ab}}{^{28}\mathrm{S}i^t - ^{28}\mathrm{S}i_{ab}}\right) \times [\mathrm{SiO}_2]^{t0} \tag{2}$$

where the subscript of "t0" and "t" denotes the initial experimental solution, the experimental solution sampled at time t, and "ab" the albite reactant in the experiments, respectively. Similar equations can be developed for ²⁹Si and ³⁰Si. If [SiO₂] calculated from ²⁸Si, ²⁹Si, and ³⁰Si is different, it may indicate fractionation during albite dissolution. If [SiO₂] calculated from isotopic fractions (IX method) is higher than [SiO₂] from Si elemental analysis (e.g., the Mo-blue method and isotope dilution method), it may indicate precipitation may have occurred during the experiment.

The isotope dilution (ID) method was used in this study in order to measure elemental silicon concentrations. A spike solution with known elemental Si concentrations and Si isotopic fractions (denoted with subscript "spi") was mixed with the experimental solution and the mixed solution (denoted as "mix") was analyzed with MC-ICP-MS again for its Si isotope fractions. The elemental Si concentrations in the experimental solutions then can be calculated via the following equations:

$$[SiO_{2}]^{t} = \left(\frac{V_{2}}{V_{1}}\right) \left(\frac{^{28}Si_{mix} - ^{28}Si_{spi}}{^{28}Si^{t} - ^{28}Si_{mix}}\right) [SiO_{2}]_{spi}$$
(3a)

Table 2Isotopic fractions for reactants, starting solutions, and spike solutions.

	²⁸ Si	²⁹ Si	³⁰ Si	δ^{30} Si (‰)	δ^{29} Si (‰)
Amelia albite	0.9223	0.0467	0.0310	-0.11	-0.256
Evje albite	0.9223	0.0467	0.0311		
Starting solution	0.0004	0.999	0.0006		
Spike solution for ID analysis	0.9223	0.0467	0.0310		

$$[SiO_2]^t = \left(\frac{V_2}{V_1}\right) \left(\frac{^{29}Si_{mix} - ^{29}Si_{spi}}{^{29}Si^t - ^{29}Si_{mix}}\right) [SiO_2]_{spi}$$
(3b)

$$[SiO_2]^t = \left(\frac{V_2}{V_1}\right) \left(\frac{{}^{30}Si_{mix} - {}^{30}Si_{spi}}{{}^{30}Si^t - {}^{30}Si_{mix}}\right) [SiO_2]_{spi}$$
(3c)

where $[\mathrm{SiO}_2]^t$ and $[\mathrm{SiO}_2]_{spi}$ stand for silicon concentrations ($\mu\mathrm{M}$) in experimental solution and analytical spike (stock) solution, respectively. V_1 and V_2 denote volumes (mL) of experimental solution and analytical spike solution that are used to make the mixed solution (equal volume in our case), respectively. $^{28}\mathrm{Si}^t$, $^{29}\mathrm{Si}^t$, and $^{30}\mathrm{Si}^t$ stand for fractions of $^{28}\mathrm{Si}$, $^{29}\mathrm{Si}$, and $^{30}\mathrm{Si}^t$ in experimental solution, $^{28}\mathrm{Si}_{spi}$, $^{29}\mathrm{Si}_{spi}$, and $^{30}\mathrm{Si}_{spi}$ fractions of $^{28}\mathrm{Si}$, $^{29}\mathrm{Si}$, and $^{30}\mathrm{Si}^t$ in analytical spike (stock) solution, and $^{28}\mathrm{Si}_{mix}$, $^{29}\mathrm{Si}_{mix}$, and $^{30}\mathrm{Si}^t$ in the mixed solution. The analytical spike solution was prepared by diluting the purchased 1000 ppm ICP standard silicon solution (silicon in 3% HNO3 and trace HF, Fisher Scientific, Pittsburgh, PA, USA) using DI water. The resultant analytical spike stock solution for the ID method was composed of 40 μ M silicon with the isotope fraction of 0.9223 $^{28}\mathrm{Si}$, 0.0467 $^{29}\mathrm{Si}$, and 0.0310 $^{30}\mathrm{Si}$. The $[^{28}\mathrm{SiO}_2]^t$, $[^{29}\mathrm{SiO}_2]^t$, and $[^{30}\mathrm{SiO}_2]^t$ in experimental solutions are calculated by multiplying the $[\mathrm{SiO}_2]^t$ with the respective fraction of $^{28}\mathrm{Si}$, and $^{30}\mathrm{Si}$ in the solution.

Total concentrations of dissolved Si in solution [SiO₂] were also analyzed with Perkin Elmer Lambda 2S UV–visible spectrophotometer, using the molybdate blue method (Govett, 1961). The uncertainty in measured Si was less than $\pm\,5\%$ for concentrations above 4 μM . Detection limits for analyses of Si are less than 0.5 μM .

2.10. Cation analysis

Total cation concentrations of [Na⁺], [Ca²⁺], [Mg²⁺], [Al³⁺], and [K⁺] were analyzed with Inductively Coupled Plasma Quadrupole Mass Spectrometry (ICP-QMS) Agilent 7700× with the measurement uncertainty of $\pm\,5\%$ or were determined with a Perkins Elmer 5000 flame and graphite furnace AAS. Solution pHs were measured at room temperature 22.5 ($\pm\,0.5$) °C on a stirred solution using a Semi-Micro 83-01 Orion Ross Combination Electrode. The reported accuracy was $\pm\,0.02$ pH units (i.e. $\pm\,4.5\%$ in H⁺ activity).

2.11. Calculation of dissolution rates

If the amount of Si-containing secondary mineral precipitation is negligible in the experiments, the albite dissolution rate, r_{dis} ((mol·ab) m⁻² s⁻¹), can be calculated from the following equation:

$$r_{dis} = \left(\frac{1}{S_{A,ab}\nu_{ab}}\right) \left(\frac{d[SiO_2]^t}{dt}\right) \tag{4}$$

where $S_{A,ab}$ denotes the surface area of albite (m²/L) in the reactor and is usually regarded as a constant when the amount of albite dissolved is small in the experiments (e.g., <1–2%). Throughout this paper, we use BET surface area for $S_{A,ab}$. ν_{ab} is stoichiometric coefficient of silicon in the albite mineral formula.

As described above, the variable $[SiO_2]^t$ were measured with two different methods: (a) conventional analytical method (i.e., Mo-blue colorimetry); and (b) from the more precise isotope dilution method (Section 2.9).

If (a) there is no silicon isotopic fractionation during albite dissolution; (b) the Si isotope fractionation during secondary mineral precipitation has negligible effects on the isotopic composition of the experimental solution; and (c) there is only one secondary mineral,

the reaction rates of primary mineral dissolution and secondary mineral precipitation can be calculated from the following two equations, respectively:

$$r_{dis} = \frac{\left[\begin{pmatrix} ^{29}Si^t}{^{28}Si^t} \end{pmatrix} \cdot \frac{d \begin{pmatrix} ^{28}Si^t \cdot [SiO_2]^t \end{pmatrix}}{dt} - \frac{d \begin{pmatrix} ^{29}Si^t \cdot [SiO_2]^t \end{pmatrix}}{dt} \right]}{\left[\begin{pmatrix} ^{29}Si^t \\ ^{28}Si^t \end{pmatrix} \cdot ^{28}Si_{ab} - ^{29}Si_{ab} \right] \cdot \nu_{ab} \cdot S_{A,ab}}$$
 (5)

$$r_{pre} = \frac{d[\text{SiO}_2]^t}{dt} - \nu_{ab} S_{A,ab} r_{dis}}{\nu_{pre} S_{A,pre}}$$
(6)

where r_{pre} denotes rate of secondary mineral precipitation (mol m⁻² s⁻¹), ν_{pre} stoichiometric coefficient of Si in secondary mineral precipitate, $S_{A,pre}$ surface area (m²/L) of secondary mineral at time t. Note that Eq. (6) is valid only when there is one type of secondary mineral that contains Si.

In Eqs. (5) and (6), the isotopic fraction of experimental solutions is directly measured from HR-MC-ICP-MS. $[SiO_2]^t$ is either measured with the conventional (Mo-blue) method or the isotope dilution method.

2.12. Calculations of mineral saturation indices

Saturation indices of minerals were calculated with the geochemical speciation software PHREEQC 2.18.3 (Parkhurst and Appelo, 1999) using the extended Debye–Hückel equation and the thermodynamic data set of Zhu and Lu (2009).

3. Si isotope mass balance models

In order to interpret Si isotope experimental data and evaluate the various complications on rate determination, we developed the following mass balance models. Specifically, we considered (A) Si isotope fractionation during albite dissolution, (B) precipitation of a Si-containing secondary phase, and (C) Si isotope fractionation during secondary phase precipitation.

3.1. Model A: albite dissolution only

See Table 1 for all symbols and notations. Here we assume that in a batch system, the only reaction is albite dissolution. From any time interval Δt from t to t+1 when the rate of albite dissolution is constant, the 28 Si fractions in the experimental solutions will change according to the mass balance,

$$\begin{cases} [SiO_2]^{t+1} = \nu_{ab} r_{ab}^{t} \Delta t + [SiO_2]^t \\ [^{28}SiO_2]^{t+1} = \nu_{ab}^{28} Si_{ab} r_{ab}^{t} \Delta t + {^{28}Si}^t [SiO_2]^t \\ [^{29}SiO_2]^{t+1} = \nu_{ab}^{29} Si_{ab} r_{ab}^{t} \Delta t + {^{29}Si}^t [SiO_2]^t \end{cases}$$
(7)

$$\begin{cases} {}^{28}\text{Si}^{t+1} = \frac{\nu_{ab}{}^{28}\text{Si}_{ab}r_{ab}^{\prime t}\Delta t + {}^{28}\text{Si}^{t}[\text{SiO}_{2}]^{t}}{\nu_{ab}r_{ab}^{\prime t}\Delta t + [\text{SiO}_{2}]^{t}} \\ {}^{29}\text{Si}^{t+1} = \frac{\nu_{ab}{}^{29}\text{Si}_{ab}r_{ab}^{\prime t}\Delta t + {}^{29}\text{Si}^{t}[\text{SiO}_{2}]^{t}}{\nu_{ab}r_{ab}^{\prime t}\Delta t + [\text{SiO}_{2}]^{t}}. \end{cases}$$
(8)

Similar mass balance equation can be written for ³⁰Si. In the above equations, the assumptions are that no Si isotope fractionation occurs during albite dissolution and that no secondary phases precipitate.

From Eq. (8), if ${}^{28}Si_{ab}$, $[SiO_2]^t$, and ${}^{28}Si^t$ are measured, ${}^{28}Si^{t+1}$ can be predicted with an assumed r'_{ab} . When an inflection point for ${}^{28}Si$ versus

t data is observed, a different r'_{ab} value must be used for different time periods (e.g., 4–20 days and 20–60 days).

Note that this model only needs one $[SiO_2]^t$ value at the beginning, e.g., day 4; the rest are predicted. We have two equations for two unknowns $(r'_{ab}, [SiO_2]^t)$ for Eq. (8), but the solutions are not unique. To obtain a unique solution, we need a $[SiO_2]^t$ value.

If ^{28}Si , ^{29}Si , and ^{30}Si data are fitted simultaneously with the same albite dissolution rate, isotopic fractionation effects on the rate determination are small. Formal evaluation of the effects of isotope fractionation on rate determination was conducted using Eqs. (32)–(34), which are derived below.

3.2. Model B: with secondary phase precipitation

Now we assume there is a "kaolinite" precipitation (or any secondary phase with a stoichiometry of Al_2Si_2). For any time interval from t to t+1 when the rates of albite dissolution and kaolinite precipitation are constant, the ²⁸Si fractions in the experimental solutions will change according to the mass balance.

$$\begin{cases} \left[SiO_{2}\right]^{t+1} = \nu_{ab}r_{ab}^{\prime t}\Delta t - \nu_{kao}r_{kao}^{\prime t} + \left[SiO_{2}\right]^{t} \\ \left[^{28}SiO_{2}\right]^{t+1} = (\nu_{ab}^{28}Si_{ab}r_{ab}^{\prime t} - \nu_{kao}^{28}Si^{t}r_{kao}^{\prime})\Delta t + {}^{28}Si^{t}\left[SiO_{2}\right]^{t} \\ \left[^{29}SiO_{2}\right]^{t+1} = (\nu_{ab}^{29}Si_{ab}r_{ab}^{\prime t} - \nu_{kao}^{29}Si^{t}r_{kao}^{\prime t})\Delta t + {}^{29}Si^{t}\left[SiO_{2}\right]^{t} \end{cases}$$
(9)

$$\begin{cases} 28 \operatorname{Si}^{t+1} = \frac{\left(\nu_{ab}^{28} \operatorname{Si}_{ab} r_{ab}^{\prime t} - \nu_{kao}^{28} \operatorname{Si}^{t} r_{kao}^{\prime t}\right) \Delta t + {}^{28} \operatorname{Si}^{t} [\operatorname{SiO}_{2}]^{t}}{\left(\nu_{ab} r_{ab}^{\prime t} - \nu_{kao} r_{kao}^{\prime t}\right) \Delta t + [\operatorname{SiO}_{2}]^{t}} \\ 29 \operatorname{Si}^{t+1} = \frac{\left(\nu_{ab}^{29} \operatorname{Si}_{ab} r_{ab}^{\prime t} - \nu_{kao}^{29} \operatorname{Si}^{t} r_{kao}^{\prime t}\right) \Delta t + {}^{29} \operatorname{Si}^{t} [\operatorname{SiO}_{2}]^{t}}{\left(\nu_{ab} r_{ab}^{\prime t} - \nu_{kao} r_{kao}^{\prime t}\right) \Delta t + [\operatorname{SiO}_{2}]^{t}} \end{cases}$$
(10)

In Eqs. (9)-(10), the assumptions are that no Si isotope fractionation occurs during albite dissolution and that kaolinite precipitation removes the prevailing Si isotope at time t (no fractionation).

When $[SiO_2]^t$ is known, Eq. (10) is reduced to a "two equations for two unknowns" problem. The two unknowns are r'_{ab} and r'_{kao} . If Model A over-predicted $[SiO_2]^{t+1}$, we can adjust the value of r'_{kao} to achieve a match between model-predicted (from Eq. (2)) and experimental $[SiO_2]^{t+1}$. The r'_{kao} value is further adjusted so that the predicted Al concentration match the experimental data.

It is tempting to use a third mass balance equation for ^{30}Si so that we have three equations and three unknowns. However, this third equation is not independent because $^{28}Si + ^{29}Si + ^{30}Si = 1$ at all times.

3.3. Model C: with isotope fractionation

3.3.1. Kinetic fractionation factor

Kinetic fractionation factor during precipitation (denoted as α'_{kao} to be distinguished from fractionation factor $\alpha_{kao-sol} = R_{kao}/R_{sol}$) used below is defined (Gruber et al., 2013),

$$\alpha'_{kao,29/28} = \frac{\binom{r'_{29,kao}}{r'_{28,kao}}}{\binom{29}{Si_{sol}}^{28}Si_{sol}}$$
(11)

where $r'_{29,kao}$ and $r'_{28,kao}$ are the rates of ²⁹Si and ²⁸Si precipitation (mol L⁻¹ s⁻¹), which are expressed as

$$r'_{29,kao} = \frac{1}{\nu_{kao}V} \frac{dn_{29Si,kao}}{dt}$$
 (12)

where *V* is the volume of solution (L), $dn_{29\text{Si},kao}/dt$ is the incorporation rate (mol/s) of ²⁹Si on the surface of the solid phase, $n_{29Si,kao}$ is the moles of ²⁹Si in kaolinite phase (mol). Similarly, for $d n_{28Si,kao}/dt$, and

Fractionation factor during dissolution (denoted as α'_{ab}) can also be defined in the same way

$$\alpha'_{ab,29/28} = \frac{\binom{r'_{29,ab}}{r'_{28,ab}}}{\binom{29}{5i_{ab}}{\binom{28}{28}Si_{ab}}}$$
(14)

where $r'_{29,ab}$ and $r'_{28,ab}$ are the rate of ²⁹Si and ²⁸Si dissolution (mol L^{-1} s⁻¹), which are can be expressed as

$$r'_{29,ab} = \frac{1}{\nu_{ab}V} \frac{dn_{29Si,ab}}{dt} \tag{15}$$

$$r'_{28,ab} = \frac{1}{\nu_{ab}V} \frac{dn_{28Si,ab}}{dt}$$
 (16)

where $dn_{29Si,ab}/dt$ is the rate of ²⁹Si released from albite surface into solution (mol s⁻¹), $n_{29Si,ab}$ is the moles of ²⁹Si in albite phase (mol). Similarly for $dn_{28Si,ab}/dt$, and $n_{28Si,ab}$.

Kinetic fractionation factors between ³⁰Si and ²⁸Si can also be defined in the same way.

3.3.2. Mass balance model with fractionation

We used the same assumptions as in Model B but now take into account of Si isotope fractionation during "kaolinite" precipitation. From any time interval from t to t+1, the ²⁸Si and ²⁹Si fractions in the experimental solutions will change according to the mass balance.

$$\begin{cases} [SiO_{2}]^{t+1} = (\nu_{ab}r_{ab}^{t} - \nu_{kao}r_{kao}^{t})\Delta t + [SiO_{2}]^{t} \\ \left[^{28}SiO_{2}\right] = (\nu_{ab}r_{28,ab}^{t} - \nu_{kao}r_{28,kao}^{t})\Delta t + {}^{28}Si^{t}[SiO_{2}]^{t} \\ \left[^{29}SiO_{2}\right] = (\nu_{ab}r_{29,ab}^{t} - \nu_{kao}r_{29,kao}^{t})\Delta t + {}^{29}Si^{t}[SiO_{2}]^{t} \end{cases}$$
(17)

$$\begin{cases} 2^{8} Si^{t+1} = \frac{\left(\nu_{ab} r_{28,ab}^{tt} - \nu_{kao} r_{28,kao}^{tt}\right) \Delta t + {}^{28} Si^{t} [SiO_{2}]^{t}}{\left(\nu_{ab} r_{ab}^{tt} - \nu_{kao} r_{kao}^{tt}\right) \Delta t + [SiO_{2}]^{t}} \\ {}^{29} Si^{t+1} = \frac{\left(\nu_{ab} r_{29,ab}^{tt} - \nu_{kao} r_{29,kao}^{tt}\right) \Delta t + {}^{29} Si^{t} [SiO_{2}]^{t}}{\left(\nu_{ab} r_{ab}^{tt} - \nu_{kao} r_{kao}^{tt}\right) \Delta t + [SiO_{2}]^{t}} \end{cases}$$

$$(18)$$

If fractionation is neglected, $r_{x,ab}t = {}^{x}Si_{ab}r_{ab}t$ and $r_{x,kao}t = {}^{x}Si_{sol}r_{kao}t$ (x = 28 or 29) and Eqs. (17) and (18) reduce to Eqs. (9) and (10) inModel B. To find the rates of dissolution and precipitation for each isotope with consideration of fractionation, the following method is used.

Assume $r'_{28,kao}$ can be expressed with r'_{kao} as a fractionation modifier

$$r'_{28,kao} = \kappa_{28,kao}^{28} Si_{sol} r'_{kao} \tag{19}$$

Similarly, $r'_{29,kao}$ and $r'_{29,kao}$ can also be expressed as,

$$r'_{29,kao} = \kappa_{29,kao}^{29} Si_{sol} r'_{kao} \tag{20}$$

$$r'_{30,kao} = \kappa_{30,kao}^{30} \text{Si}_{sol} r'_{kao}. \tag{21}$$

Divide Eqs. (20) and (21) by Eq. (19) and rearrange, we have,

$$\frac{\kappa_{29,kao}}{\kappa_{28,kao}} = \frac{r'_{29,kao}}{r'_{28,kao}}^{28} \frac{s_{isol}}{s_{ol}} = \alpha'_{kao,29/28}$$
(22)

$$\frac{\kappa_{30,kao}}{\kappa_{28,kao}} = \frac{r'_{30,kao}}{r'_{28,kao}} \frac{^{28}Si_{sol}}{^{30}Si_{sol}} = \alpha'_{kao,30/28}.$$
 (23)

The sum of the precipitation rate of all three individual isotopes must equal the overall rate of precipitation,

$$r'_{28,kao} + r'_{29,kao} + r'_{30,kao} = r'_{kao}. (24)$$

Substitute Eqs. (19)–(21) to Eq. (24), we have

$$\kappa_{28,kao}^{28}Si_{sol} + \kappa_{29,kao}^{29}Si_{sol} + \kappa_{30,kao}^{30}Si_{sol} = 1.$$
 (25)

Rearrange Eqs. (22), (23) and (25), and solve for all three modifiers,

$$\kappa_{28,kao} = \frac{1}{{}^{28}\text{Si}_{sol} + {}^{29}\text{Si}_{sol}\alpha'_{kao,29/28} + {}^{30}\text{Si}_{sol}\alpha'_{kao,30/28}}$$
(26)

$$\kappa_{29,kao} = \frac{\alpha'_{kao,29/28}}{{}^{28}Si_{sol} + {}^{29}Si_{sol}\alpha'_{kao,29/28} + {}^{30}Si_{sol}\alpha'_{kao,30/28}}$$
(27)

$$\kappa_{30,kao} = \frac{\alpha'_{kao,30/28}}{{}^{28}Si_{sol} + {}^{29}Si_{sol}\alpha'_{kao,29/28} + {}^{30}Si_{sol}\alpha'_{kao,30/28}}.$$
 (28)

Using Eqs. (26)–(28), we can find the precipitation rate of each iso-

$$r'_{28,kao} = \frac{{}^{28}Si_{sol}}{{}^{28}Si_{sol} + {}^{29}Si_{sol}\alpha'_{kao,29/28} + {}^{30}Si_{sol}\alpha'_{kao,30/28}}r'_{kao}$$
(29)

$$r'_{29,kao} = \frac{^{29} Si_{sol} \alpha'_{kao,29/28}}{^{28} Si_{sol} + ^{29} Si_{sol} \alpha'_{kao,29/28} + ^{30} Si_{sol} \alpha'_{kao,30/28}} r'_{kao}$$
(30)

$$r'_{30,kao} = \frac{{}^{30}Si_{sol}\alpha'_{kao,30/28}}{{}^{28}Si_{sol} + {}^{29}Si_{sol}\alpha'_{kao,29/28} + {}^{30}Si_{sol}\alpha'_{kao,30/28}}r'_{kao}. \tag{31}$$

The dissolution rate of each isotope can also be found in the same way, and the results can be expressed as Eqs. (32)–(34)

$$r'_{28,ab} = \frac{{}^{28}Si_{ab}}{{}^{28}Si_{ab} + {}^{29}Si_{ab}\alpha'_{ab,29/28} + {}^{30}Si_{ab}\alpha'_{ab,30/28}}r'_{ab}$$
(32)

$$r'_{29,ab} = \frac{{}^{29}Si_{ab}\alpha'_{ab,29/28}}{{}^{28}Si_{ab} + {}^{29}Si_{ab}\alpha'_{ab,29/28} + {}^{30}Si_{ab}\alpha'_{ab,30/28}}r'_{ab}$$
(33)

$$r'_{30,ab} = \frac{{}^{30}Si_{ab}\alpha'_{ab,30/28}}{{}^{28}Si_{ab} + {}^{29}Si_{ab}\alpha'_{ab,20/28} + {}^{30}Si_{ab}\alpha'_{ab,30/28}}r'_{ab}.$$
 (34)

The above three models (A, B, C) were programmed into an Excel® spreadsheet and used to evaluate the isotope experimental data. r'_{ab} was first adjusted until the visually best match for the *Si versus t experimental data was found. The best fit rates were then found with a MatLab® script using the least squares method.

4. Experimental results

4.1. The Si isotope fractionation during albite dissolution

In order to find out silicon isotope fractionation during albite dissolution, we performed no-doping experiments (dissolution of albite into DI water). See Section 2.3 for experimental details. The results of these experiments are shown in Table 3 and Figs. 2 and 3.

 $\delta^{30}Si_{sol}$ and $\delta^{29}Si_{sol}$ of the experimental solutions ranged from -2.976 to 0.694% and -1.784 to 0.338%, respectively, but most $\delta^{30}Si_{sol}$ and $\delta^{29}Si_{sol}$ values are lower than $\delta^{30}Si_{ab}$ and $\delta^{29}Si_{ab}$ (Fig. 2), documenting lighter Si isotopes were preferentially released into solution from albite. The apparent Si isotope enrichment factor ($^{30}\epsilon_{sol-ab}$) ranged from -2.870 to 0.804%, and averaged at $-0.995 \pm 1.161\%$, which is typical for terrestrial surficial systems (Opfergelt and Delmelle, 2012). These results are consistent with previous findings in the literature (see compilations in Opfergelt and Delmelle, 2012).

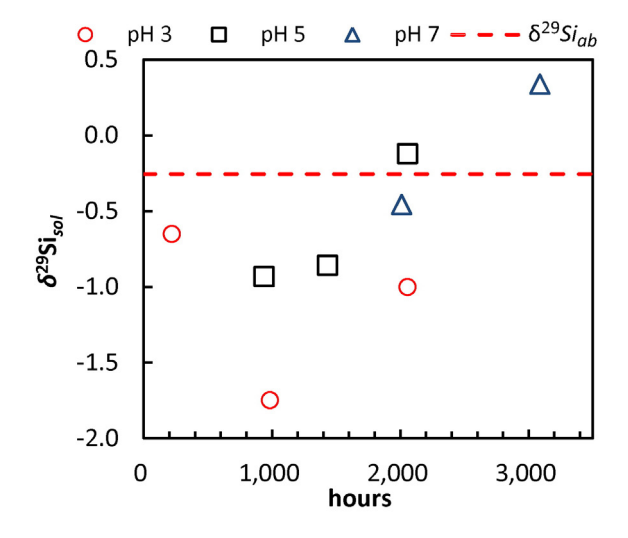
Additionally, the extent of the fractionation appears to depend on pH and reaction time. Larger fractionation occurred at lower pH. The $^{30}\varepsilon_{sol-ab}$ at pH 3 is about 1‰ more negative than that at pH 5. With longer reaction time, the experimental solutions became isotopically heavier as dissolution proceeded (Figs. 2, 3). After ~3000 h of reaction, the fractionation pattern was reversed. A similar trend with reaction time was found in dissolution of basalt glass (Ziegler et al., 2005). The reason for this behavior is unclear but precipitation of secondary phases can result in a positive δ^{30} Si shift in the solution because of the preferential incorporation of 28 Si into secondary phases (Ziegler et al., 2005; Opfergelt and Delmelle, 2012).

Therefore, our experimental data show fractionation of Si isotopes during albite dissolution, with lighter isotopes preferentially released from albite. The fractionation is larger than previously realized and can be significant in understanding silicon biogeochemical cycles. However, as shown below, the fractionation only has negligible effects on determining the reaction rates using the isotope doping method.

4.2. Si isotope data and dissolution rates

Fig. 1b shows dissolution features of the albite after the experiments. Figs. 4, 5, and 6 show that the measured ^{28}Si and ^{30}Si fractions increased and ^{29}Si decreased rapidly after the initial contact between the albite powder and aqueous solutions. The changes were much slower after 3–4 days, and developed into monotonic trends all the way to the end of experiments, up to 270 days later. The analytical precision of isotope fraction to $\pm\,0.0005$ to $\pm\,0.001$ allowed the changes of Si isotopic fraction at all sampling intervals to be easily detected. Below, we will only discuss reaction rates after 3–4 days. The rapid changes of isotopes between 0 and 4 days will be described in another contribution. Experimental solution pH and other conditions are presented in Table 4.

At pH 3 (Exp #1-1, Fig. 4), the albite dissolution experiment lasted 270 days. Fractions for all three Si isotopes from day 4 to day 270 were fitted with a single albite dissolution rate of $10^{-11.75}$



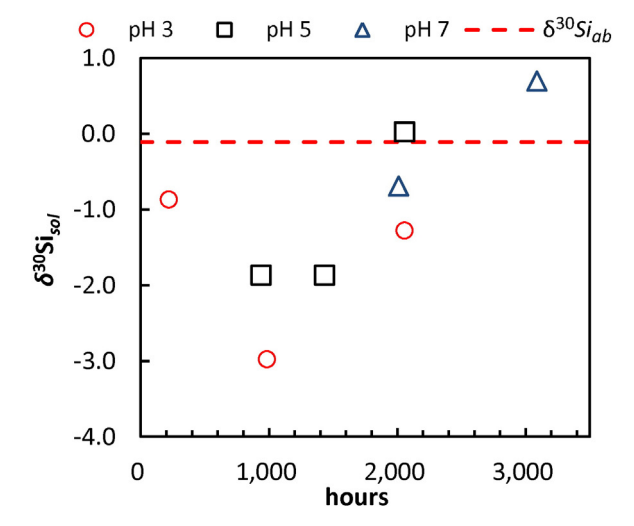


Fig. 2. $\delta^{29} Si_{sol}$ and $\delta^{30} Si_{sol}$ of experimental solutions with reaction time. The dashed lines are values for Amelia albite ($\delta^{30} Si - 0.11\%$ and $\delta^{29} Si - 0.256\%$).

 (1.78×10^{-12}) mol m⁻² s⁻¹ (red lines in Fig. 4). The surface area used in the normalization was the BET surface area of the reactant and we assumed that surface area did not change during the experiments. In all experiments, the amount of albite dissolved was less than 3%. As shown in Fig. 1b, an increase of surface area during the experiment is expected, and the use of a constant surface area here introduces some errors for rate determination. The predicted Si isotope fractions (the red lines) were calculated from Model A (see Section 3.1). Dissolution rates calculated from Eq. (5), based on intervals between two consecutive sampling points, are shown as a function of reaction time (Fig. 7).

Table 3 a Fractionation factor (α) , δ , Δ and ε bet ween solution samples and albite.

Sample	pН	Time (h)	$\alpha_{sol-ab(29/28)}$	$\alpha_{sol-ab(30/28)}$	$\delta^{29} Si_{sol}$	$\delta^{30} Si_{sol}$	$\Delta^{29} Si_{sol-ab}$	$\Delta^{30} Si_{sol-ab}$	$^{29}\varepsilon_{sol-ab}$	$^{30}\varepsilon_{sol-ab}$
1-0 #6	3	221.0	0.99960	0.99924	-0.651	-0.869	-0.395	-0.759	-0.395	-0.759
1-0 #7	3	985.9	0.99851	0.99713	-1.748	-2.976	-1.492	-2.866	-1.494	-2.870
1-0 #9B	3	2057.8	0.99925	0.99883	-1.003	-1.276	-0.747	-1.166	-0.747	-1.167
2-0 #7	5	938.2	0.99932	0.99825	-0.934	-1.865	-0.678	-1.755	-0.678	-1.756
2-0 #8	5	1434.4	0.99940	0.99824	-0.858	-1.866	-0.602	-1.756	-0.602	-1.758
2-0 #9B	5	2058.2	1.00013	1.00013	-0.122	0.024	0.134	0.134	0.134	0.134
3-0 #9B	7	2011.0	0.99980	0.99942	-0.457	-0.694	-0.201	-0.584	-0.201	-0.585
3-0 #10	7	3090.5	1.00059	1.00080	0.338	0.694	0.594	0.804	0.594	0.804

^a Symbols are shown in Table 1.

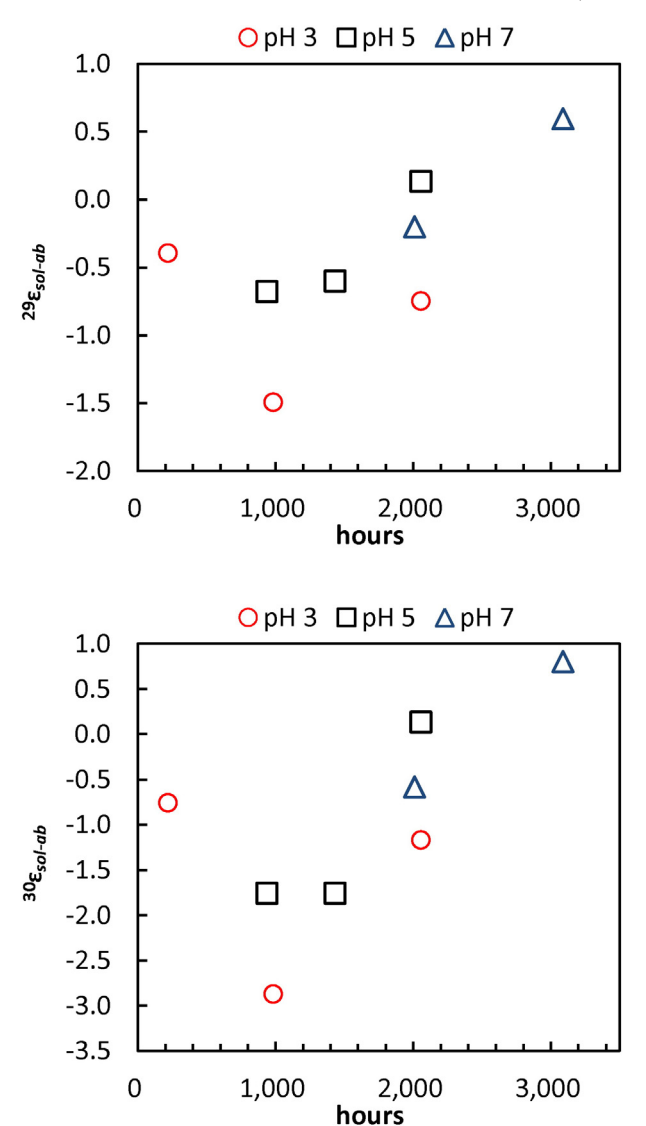


Fig. 3. Apparent $^{29}\varepsilon_{sol-ab}$ and $^{30}\varepsilon_{sol-ab}$ values from no-doping experiments.

Four experiments (Exp #4-1, 5-1, 6-1, and 7-1) were conducted at pH ~5 with various initial $[SiO_2]^{t0}$ and therefore different saturation states (Fig. 5), for up to 60 days. The three experiments (Exp #4-1, 5-1, 6-1) without kaolinite seeds showed a decrease of albite dissolution rates at ~10 days and the one with kaolinite seeds (Exp #7-1) showed a decreased rate at ~20 days. Two different albite dissolution rates for two different time periods appears to be needed to fit this data set. However, all three Si isotopes were fitted with the same dissolution rate simultaneously.

Dissolution rates calculated from Eq. (5) are similar to those reported in the literature (Fig. 7). However, our experiments lasted longer than the times to steady state found in earlier studies (e.g., Knauss and Wolery, 1986) (Fig. 7b). $\Delta G_{r,ab}$ for the experiments were calculated from geochemical modeling (see Section 2.12) and are plotted against the dissolution rates in Fig. 8. They range from -67 to -25 kJ/mol and mostly fall in the range of the "far from equilibrium rate plateau" (Zhu, 2009). The experimental solutions were consistently undersaturated with respect to kaolinite and gibbsite.

Experiment 3-1 was conducted at pH 7.6, and it lasted 127 days. The ${}^{x}Si^{t}$ versus t was fitted with one albite dissolution rate and all three isotopes were fit simultaneously.

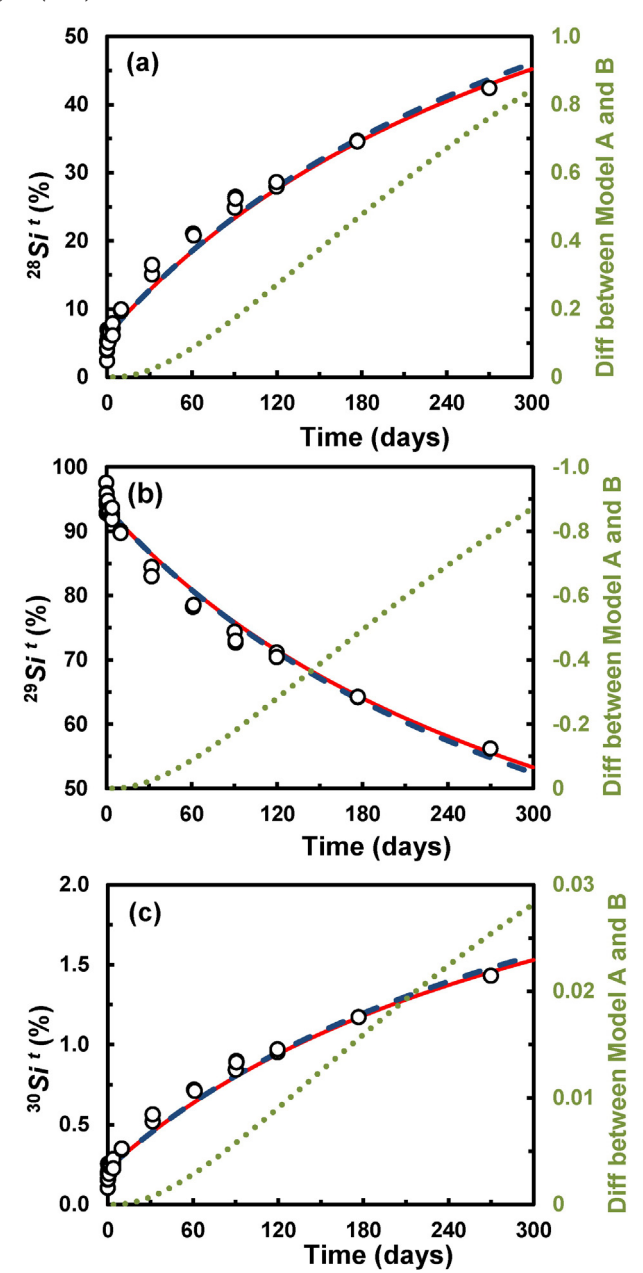


Fig. 4. Si isotope fractions in aqueous solutions from Exp #1-1 (22 °C and pH 3) versus time. The circles denote MC-ICP-MS measurements. Red lines are the isotope ratios predicted by the mass balance Model A (albite dissolution only). The blue dashed lines assume albite dissolution and simultaneous precipitation of a secondary phase with a stoichiometry of Al_2Si_2 but no Si isotopic fractionation during precipitation (Model B). The model for Si isotope fractionation (Model C) overlaps with the blue lines and is not visible. A single rate value of $10^{-11.75}$ mol m $^{-2}$ s $^{-1}$ was used in all models from day 4 to 270. The green dotted line corresponding to the right hand Y-axis and shows the difference between isotope fractions predicted by Model A and B ($^{\times}Si^{\dagger}_{B} - ^{\times}Si^{\dagger}_{A}$). (For interpretation of the references to color in this figure legend, the reader is referred to the web version of this article.)

4.3. Methods of rate calculations and precisions of rate measurements

Here we compare various methods of utilizing the isotope data to determine reaction rates and recommend the method of forward modeling (see Model A, B, and C in Section 3) to retrieve rates from isotope data. The advantages of the forward modeling method over rate equation method (i.e., Eq. (5)) can be illustrated by using Model A. In the experiments, the slopes of the $^{29}Si^t$ or $^{28}Si^t$ versus t curves (Figs. 4 and 6) are a function of only two variables: initial Si concentrations (or $[SiO_2]$ at the beginning of any time interval of interest) and albite

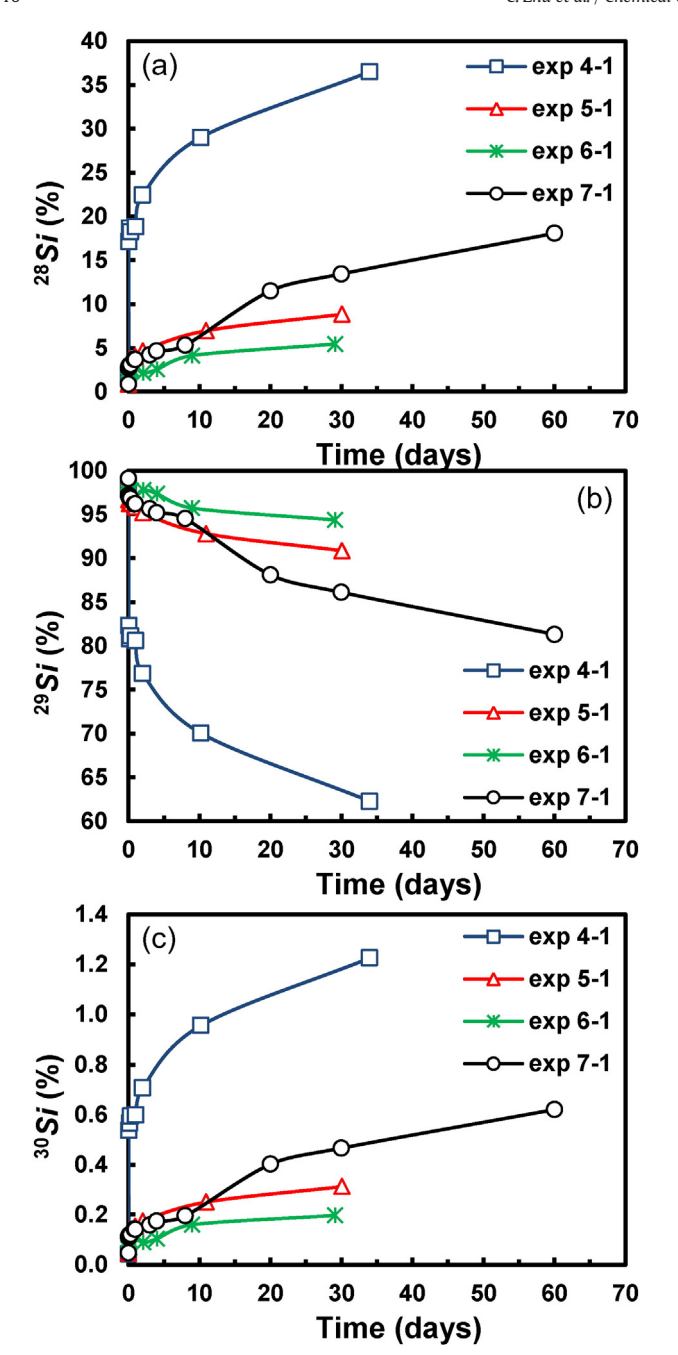


Fig. 5. Si isotope fractions versus time for Exp #4-1, Exp #5-1, Exp #6-1, and Exp #7-1. All experiments were carried out at 22 °C and pH \sim 5 with initial 29 SiO $_2$ concentrations of 4.14, 31.76, 80.49 and 31.87 μ M L $^{-1}$, respectively.

dissolution rates. This relationship was demonstrated mathematically in Section 3.1. For any time interval between t to t+1, based on mass balance, we have Eq. (35),

$${}^{x}Si^{t+1} = \frac{\nu_{ab}{}^{x}Si_{ab}r_{ab}^{rt}\Delta t + {}^{x}Si^{t}[SiO_{2}]^{t}}{\nu_{ab}r_{ab}^{rt}\Delta t + [SiO_{2}]^{t}}$$
(35)

where the symbols are explained in Table 1.

In our experiments, the Si isotope compositions of reactant albite and the solution, and the Si concentrations at time t, $[SiO_2]^t$, were measured. Therefore, there is only one degree of freedom for fitting experimental data with the albite dissolution rate for a time period when the rate is constant. In other words, a xSi versus t curve completely

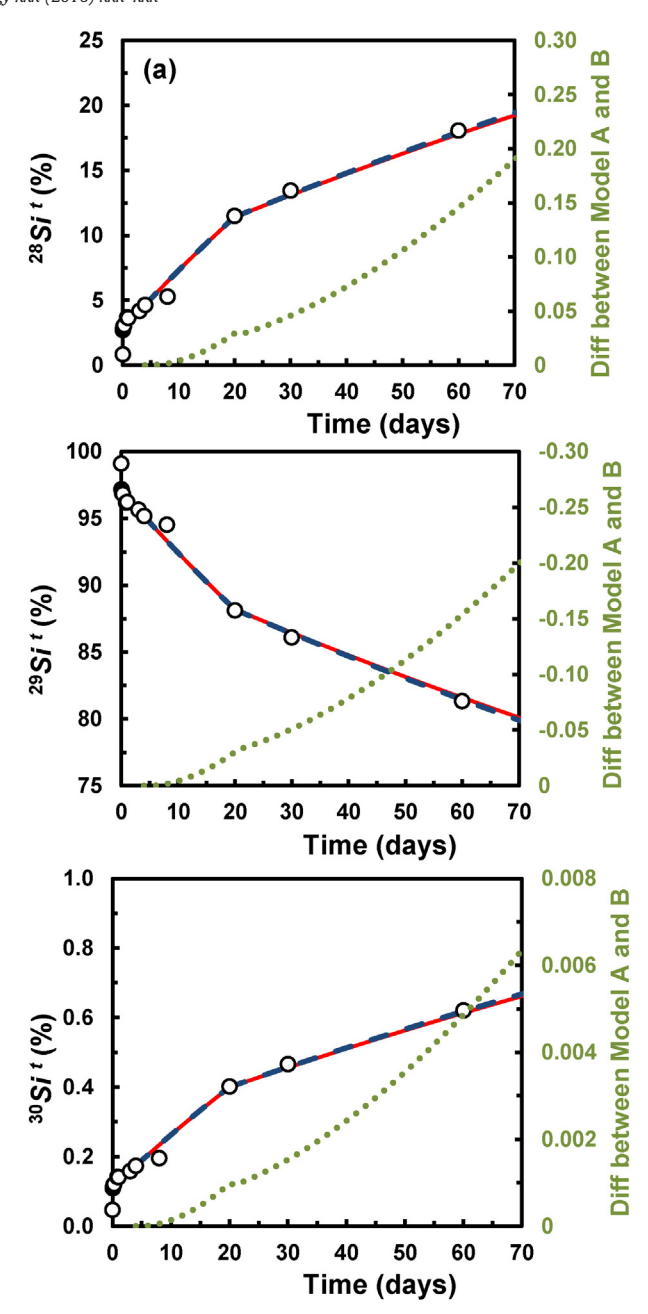


Fig. 6. Si isotope fractions in Exp #7-1 aqueous solutions (22 °C and pH ~5, seeded with kaolinite) versus time. The red lines are from Model A, which assumes albite dissolution only. The blue dashed lines are from Model B, which assumes albite dissolution and simultaneous kaolinite precipitation. The predicted lines from Model C, with Si isotope fractionation during dissolution and precipitation lies under with the blue lines and hence not visible. The green dotted line shows the difference between predicted isotope fractions between Models A and B ($^{\kappa}$ Si t B $^{-\kappa}$ Si t A). (For interpretation of the references to color in this figure legend, the reader is referred to the web version of this article.)

constrains the albite dissolution rate; a change of rates with time is reflected by the changes of slopes or tangents. Each ^{x}Si versus t curve presents one equation for one unknown for a given time period. One does not have much leeway to choose when rates change; choices to fit the data are very limited.

If $[SiO_2]^t$ is not precisely known, the albite dissolution rate fitted from one xSi versus t curve will not result in a match on another xSi versus t curve. For example, if albite dissolution between 4 and 270 days at pH 3 is fitted with 28Si versus t data (Fig. 4a) but $[SiO_2]$ at day 4 were not measured accurately, we would not see a match between the predicted ${}^{29}Si$ versus t data on Fig. 4b. In other words, the ${}^{28}Si$ versus t data and ${}^{29}Si$ versus t data provide two equations for two unknowns for a given time

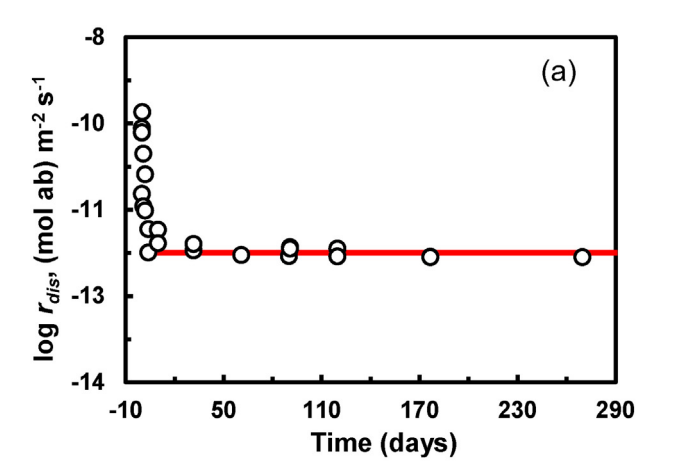
Table 4Experimental conditions and results.

Exp	Dur (days)	рН	Initial [SiO ₂] (μΜ)	SI ab	SI kao	SI gbs	S-T r_{dis} (mol ab) m ⁻² s ⁻¹	L-T r_{dis} (mol ab) m ⁻² s ⁻¹	S-T r_{pre} (mol kao) L ⁻¹ s ⁻¹	L-T r_{pre} (mol kao) L ⁻¹ s ⁻¹
1-1	270.0	3.00-3.15	56.84	-12.3	-6.42	-4.49	1.78×10^{-12}	1.78×10^{-12}	1.15×10^{-13}	6.37×10^{-13}
3-1	127.8	7.60	31.50	-4.2	3.08	0.76	_	1.86×10^{-13}	_	1.23×10^{-13}
4-1	34.0	5.15-5.83	4.14	-10.9	2.44	-1.29	6.92×10^{-13}	3.55×10^{-13}	3.58×10^{-15}	3.58×10^{-15}
5-1	30.1	5.32-5.55	31.76	-6.9	0.78	-0.40	1.26×10^{-12}	5.01×10^{-13}	7.14×10^{-14}	7.14×10^{-14}
6-1	29.1	5.27-5.55	80.49	-4.4	0.69	-0.91	1.78×10^{-12}	6.31×10^{-13}	1.13×10^{-13}	1.13×10^{-13}
7-1	60.0	5.20-5.70	31.87	-4.7	5.23	1.76	1.78×10^{-12}	7.94×10^{-13}	1.17×10^{-13}	1.17×10^{-13}

Solid:solution is 0.25:100 g in all experiments; short-term (S-T) for Exp 1-1, 4-1, 5-1, 6-1, and 7-1 are 4-150, 2-10, 1-10, 1-10, and 4-20 days, respectively; long-term (S-T) for Exp 1-1, 3-1, 4-1, 5-1, 6-1, and 7-1 are 150-270, 60-128, 10-34, 10-30, 10-30, 20-60 days, respectively. SI (saturation indices) represent at the end of experiments. IX stands for elemental Si concentrations calculated from isotopic mixing assuming no secondary mineral precipitation. ID stands for isotope dilution method of measuring [SiO₂].

interval. As stated earlier, the mass balance Model A assumes that no fractionation of Si isotopes and no the precipitation of a Si-containing secondary phase. If these assumptions were not valid, we would have seen that the albite dissolution rates fitted with one isotope did not match the other two isotopes.

Experience from forward mass balance modeling during this study showed that the ${}^{x}Si$ versus t experimental data determined albite dissolution rates with high precision. This conclusion was confirmed by sensitivity analysis. Using Eq. (35), we calculated ${}^{28}Si^{r}$ by varying albite



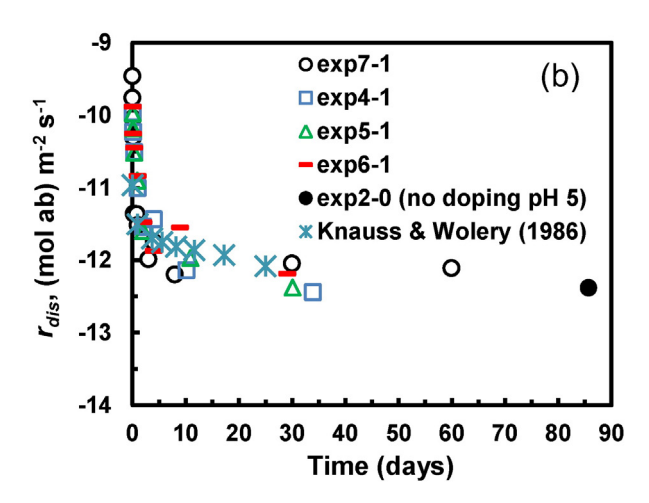


Fig. 7. (a). Albite dissolution rates for Exp #1-1 (22 °C pH 3) versus time compared to rates calculated from Eq. (5). The red line is based on the best fit rate ($10^{-11.75}$ mol m $^{-2}$ s $^{-1}$) from of Si isotope fraction data (Fig. 4) from day 4 to day 270. (b) Albite dissolution rates for experiments Exp #4-1, Exp #5-1, Exp #6-1, and Exp #7-1 (all at 22 °C, pH 5 but with different initial 29Si concentrations) versus time. The symbol * stands for rates measured by Knauss and Wolery (1986) using dissolved Si concentrations. (For interpretation of the references to color in this figure legend, the reader is referred to the web version of this article.)

dissolution rates \pm 5% from the best fit rate of $10^{-12.10}$ mol m $^{-2}$ s $^{-1}$. The predicted fraction would be 0.1830 at day 60, 0.0024 larger than the experimental datum of 0.1806 (Fig. 9a). Varying the rate by \pm 10% resulted in >0.0053 or <0.0073 offset from the experimental value, meaning that the predicted values would be 0.1806 + 0.0053 = 0.1859, or 0.1806–0.0073 = 0.1733, respectively (Fig. 9a). Silicate dissolution rates determined based on measured Si release rate carry large errors to $n \times 100\%$ (Hellmann and Tisserand, 2006; Gruber et al., 2013). Our experimental data show that the Si isotope doping technique is a highly precise way to determine silicate reaction rates.

On the other hand, the use of the rates calculated from Eq. (5) requires the knowledge of $d[^{28}\mathrm{SiO}_2]/dt$ and $d[^{29}\mathrm{SiO}_2]/dt$, which in practice is $\Delta[^{28}\mathrm{SiO}_2]/\Delta t$ and $\Delta[^{29}\mathrm{SiO}_2]/\Delta t$ between two consecutive sampling steps. The choice of the two consecutive time steps could be arbitrary. The use of Eq. (5) also requires a knowledge of $[\mathrm{SiO}_2]^t$ for all samples. The calculated rates carry large uncertainties, up to $n \times 100\%$ (Gruber et al., 2013). Furthermore, the effects of isotopic fractionation during albite dissolution and secondary phase precipitation cannot be evaluated. This practice is not recommended.

4.4. Dissolution rate determination while a secondary phase is precipitating

Here we show that the albite dissolution rates from our experiments are valid even while a Si-containing secondary phase was precipitating.

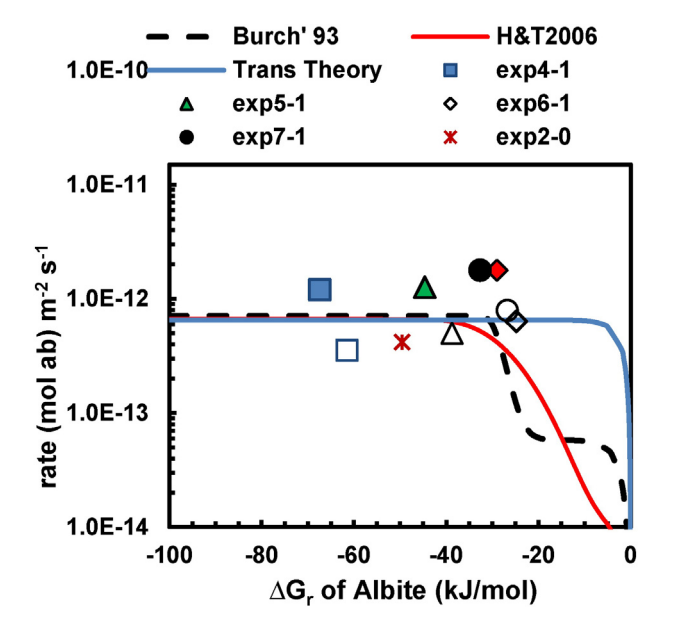


Fig. 8. Albite dissolution rates at pH~5 versus Gibbs free energy of reaction. The blue line is based on a linear rate law. The black dashed line was calculated using the "Burch rate law" and the rate parameters from Burch et al. (1993). The black line was using the "Burch rate law" and the rate parameters from Hellmann and Tisserand (2006). The solid symbols are rates based on data taken from 3 to 10 days and the open symbols are rates based on data taken from 10 to 60 days.

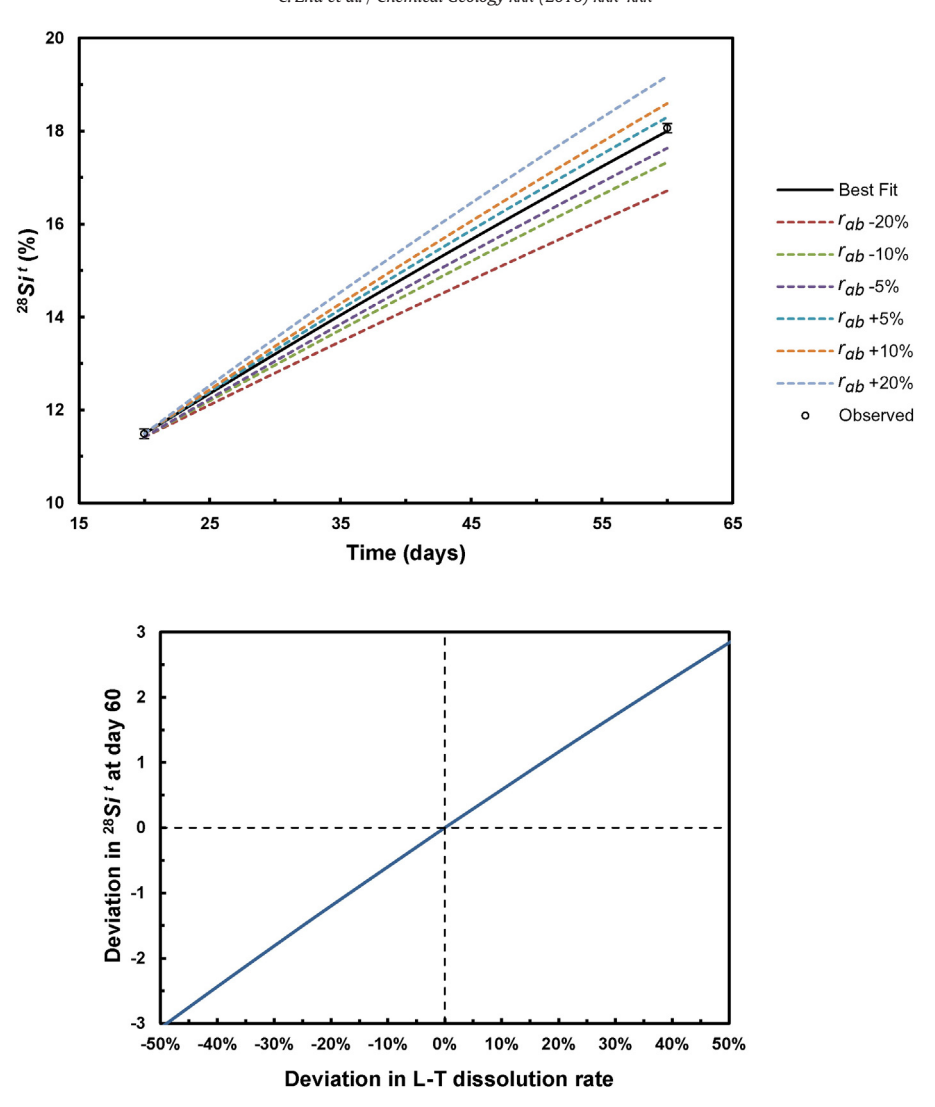


Fig. 9. Sensitivity analysis for the determination of dissolution rates. (a) 28 Si fraction expected at day 60 based on differences in the rate ranging from -20% to +20% of the measured value. The solid line shows the rate measured in Exp #7-1. The vertical error bars represents an analytical uncertainty of ± 0.001 (2σ) in isotope fraction. (b) Graph of the change in 28 Si fraction (difference in rates/best fit rate) at day 60 versus the error in determining dissolution rate.

A common challenge for measuring silicate dissolution rates is avoiding precipitation of a secondary phase during the experiments. This is particularly true for experiments in the near equilibrium region, where solute concentrations are high and for experiments in the circumneutral pH range where the solubility of secondary phases is low. For our experiments, speciation-solubility modeling, using the thermodynamic data compiled by Zhu and Lu (2009), showed that the solutions in the experiments at pH 5 #5-1, 6-1, and 7-1 (40–100 μ M Si) were supersaturated with respect to kaolinite while those in the experiment with low initial [SiO2] (~4 μ M Si) were not. The Si and Al concentration data also indicate secondary precipitation for Exp #7-1 (Fig. 10) and Exp #1-1 (Fig. 11).

To evaluate the interference of secondary phase precipitation on our determination of dissolution rates, we predicted xSi versus t using a second mass balance model (Model B, see Section 3.2), which considers simultaneous albite dissolution and precipitation of a secondary phase with a stoichiometry of Al_2Si_2 per mole solid. In Model B, we assumed no Si isotope fractionation during precipitation. We also assumed that the precipitate incorporated the prevailing Si isotopic composition of experimental solution at the time of precipitation. The broken blue lines in Figs. 4 and 6 show the modeling results (Model B). The differences between the blue and red lines are negligible, and the two lines mostly overlap. The differences between the results from the two

models are also plotted as green dotted lines on the second Y-axis on the right hand side. The figures showed that the errors from neglecting secondary phase precipitation are cumulative and increase with time or with the amount of secondary phase precipitated. For Exp #1-1, the errors for predicted ^{28}Si and ^{29}Si accumulated to $\sim\pm$ 0.008 at day 270, and for Exp #7-1, to $\sim\pm$ 0.002 at day 70. These errors exceed analytical uncertainty for isotopic fractionation of \pm 0.0005 to \pm 0.001.

The differences between the two models was due to removal of SiO₂ which changed the Si concentrations used in the next time step calculation. That caused slightly different Si isotopic ratios for the aqueous solutions. Precipitation removed more ²⁹Si than ²⁸Si from solution because of its higher abundance in the doped solution even though the secondary phases preferentially incorporate lighter Si isotopes (see below). Neglecting precipitation causes under prediction of ²⁸Si fraction (the blue lines lie slightly above the red line in Figs. 4a and 6a) and over predicts ²⁹Si (the blue lines lie slightly under the red line in Figs. 4b and 6b). However, the resulting error is still small for rate determination. As shown in Section 4.3, for Exp #7-1, an error of $\sim \pm 0.0024$ at day 60 in isotope fractions corresponds to error ~5% in albite dissolution rate determination. Therefore, for Exp #7-1, the error would be <5%. If the amount of precipitation relative to the Si pool in the aqueous solution is larger, we expect larger uncertainties.

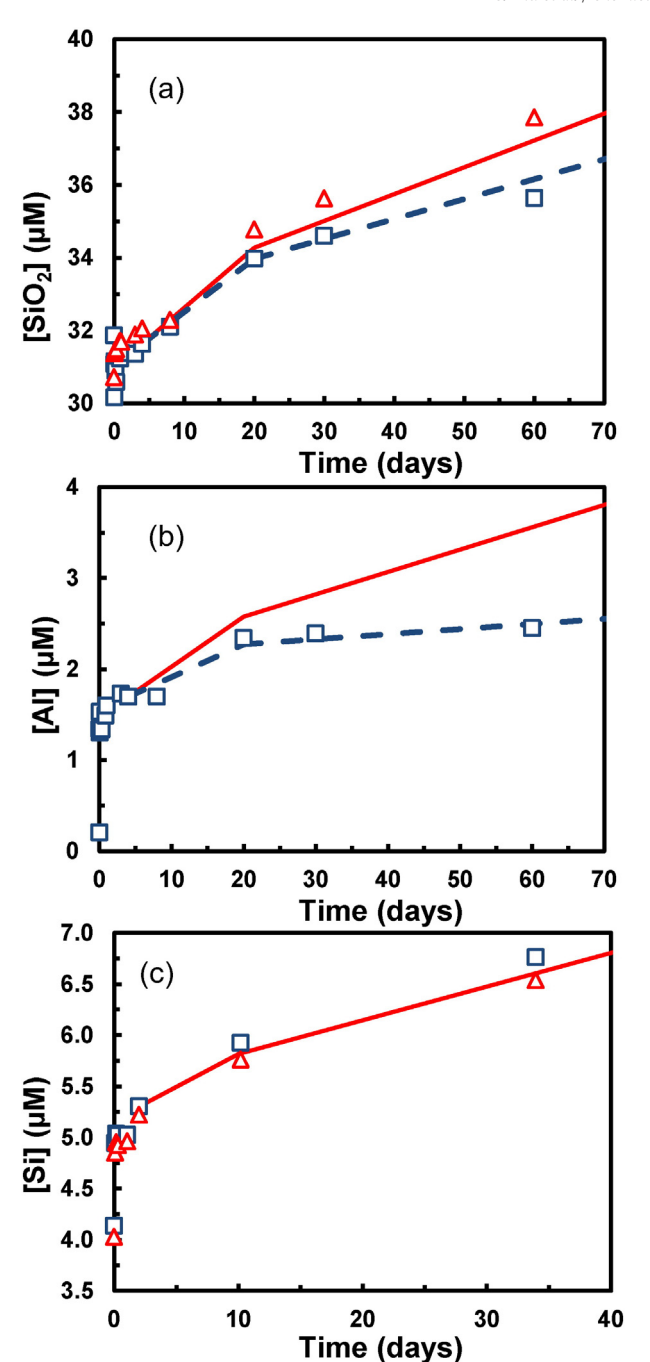


Fig. 10. (a) SiO_2 concentration versus time for Exp #7-1. (b) Al concentration versus time for Exp #7-1. (c) SiO_2 concentration versus time for Exp #4-1. The red lines are predicted using Model A, which assumes albite dissolution only. The blue broken line is based on Model B, which assumes that "kaolinite" precipitates while albite dissolves. (For interpretation of the references to color in this figure legend, the reader is referred to the web version of this article.)

However, we did not ignore secondary phase precipitation in this study. Model B corrected the possible effects of precipitation on isotopic compositions of the solution. Below (Section 4.6), we show that the amount of secondary phase precipitation can be found from the difference between [SiO₂] predicted from isotope mixing and the [SiO₂] measured using the Mo-blue and isotope dilution methods. In conclusion, the errors from the precipitation of a Si-containing secondary phase are small, but these errors are eliminated by combining the isotope and Si concentration data.

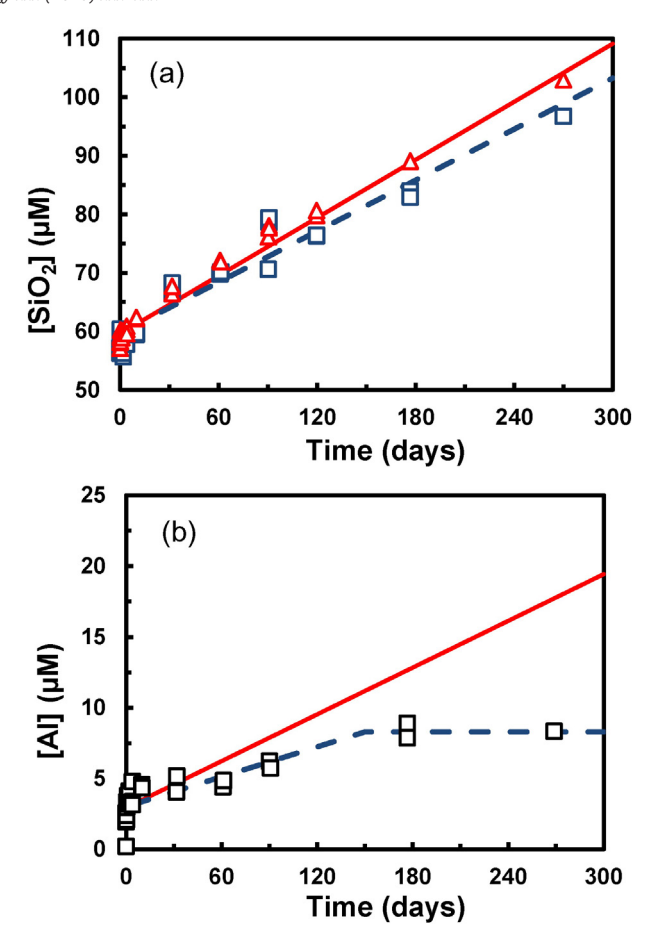


Fig. 11. (a) SiO_2 concentration versus time for Exp 1-1. The red triangles show calculated from isotopic mixing and the blue squares are $[SiO_2]^f$ measured using the isotope dilution method. (b) Al concentrations versus time. The red lines represent the concentrations predicted by Model A using an albite dissolution rate of $10^{-11.78}$ mol m $^{-2}$ s $^{-1}$. The blue broken line represents concentrations calculated using Model B, which assumes albite dissolution with simultaneous kaolinite precipitation. (For interpretation of the references to color in this figure legend, the reader is referred to the web version of this article.)

4.5. Effects of Si isotope fractionation on rate determination

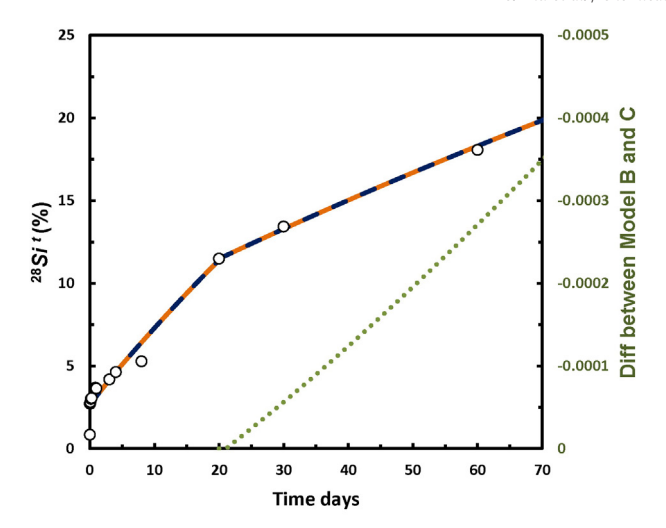
Alteration of the Si isotopic ratios in the solution can also come from Si isotopic fractionation during dissolution and precipitation. Zhu and co-workers analyzed the Si isotopes of feldspars and smectite in the Navajo sandstone at Black Mesa, Arizona, USA, and showed $\Delta^{30} \text{Si}_{fsp-clay}$ of 0.4% ($\Delta^{30} \text{Si}_{fsp-clay} = \delta^{30} \text{Si}_{fsp} - \delta^{30} \text{Si}_{clay}$), with the lighter isotopes preferentially incorporated into clays (Georg et al., 2009). Ziegler et al. (2005) found fractionation factors $^{30} \varepsilon_{solid-sol} = -2\%$ for kaolinite in the field and $^{30} \varepsilon_{solid-sol} = -1.8\%$ for allophane at 90 °C in experiments. The $^{29} \varepsilon_{solid-sol}$ can be estimated using Eq. (36)

$$^{29}\varepsilon_{\text{solid-sol}} = \beta^{30}\varepsilon_{\text{solid-sol}} \tag{36}$$

where $\beta=0.5092$ (Opfergelt and Delmelle, 2012). If similar fractionation occurred in our albite-secondary phase system, it would result in enrichment of 29 Si and 30 Si and depletion of 28 Si in solution.

We evaluated the possible effects of isotopic fractionation on the *Si^t (and hence the measured rates) using Model C which included a fractionation factor ϵ in the mass balance equations (see Section 3.3). The exact kinetic fractionation factor α' in Eq. (11) is difficult to obtain. Our evaluations below therefore used bounding parameters to see the potential effects.

The predicted ${}^{x}Si$ using ${}^{29}\epsilon{}^{\prime}{}_{kao\text{-}sol} = -1.0\%$ (${}^{30}\epsilon{}^{\prime}{}_{kao\text{-}sol} = -2\%$) completely overlap with the blue lines (Model B, without fractionation,



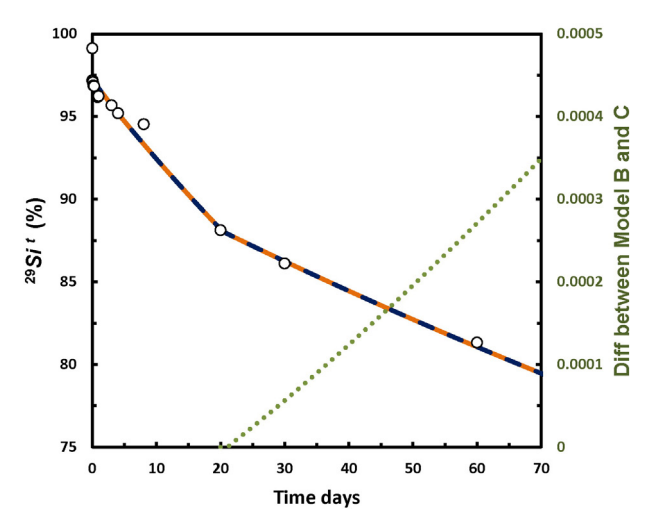


Fig. 12. The differences (in fraction, show as green dotted lines) between Models B and C in (a) 28 Sf and (b) 29 Si with a fractionation factor 29 ε $'_{kao} = -1\%$, using data from Exp #7-1 (black circles) as an example. The lines for Model B (blue dashed line) and Model C (orange solid line) overlap with each other for the entire experiment. (For interpretation of the references to color in this figure legend, the reader is referred to the web version of this article.)

Fig. 12). The errors due to neglecting isotopic fractionation during precipitation cumulate with time, but error in $^{28}Si^t$ at day 60 is less than 0.000003 in the example of Exp #7-1, which is within analytical uncertainty of \pm 0.0005–0.001. Increasing $^{29}\epsilon'_{kao\text{-}sol}$ to \pm 10% ($^{30}\epsilon'_{kao\text{-}sol}$ = \pm 20%) led to error in $^{28}Si^t$ at day 60 < 0.00003. This shows that even with a hypothetical high enrichment factor of $^{29}\epsilon'_{kao\text{-}sol}$ = \pm 10%, there are no discernable effects on rates.

The effects discussed above can be illustrated quantitatively with either the closed system Rayleigh model:

$$\delta^{30}Si_{DSi} = \delta^{30}Si_{initial} + {}^{30}\varepsilon_{kao-sol} \ln(f)$$
(37)

or the open system steady state model (Opfergelt and Delmelle, 2012),

$$\delta^{30} \operatorname{Si}_{DSi} = \delta^{30} \operatorname{Si}_{initial} - {}^{30} \varepsilon_{kao-sol} (1 - f)$$
(38)

where DSi stands for the dissolved Si and "initial" stands for t in time bracket t to t+1. Here, f is the fraction of Si that remains in the solution. In our batch experiment system, albite dissolution continues adding Si into solution and the overall Si concentrations increase. At each time step of one day, f=0.9994 for Exp #7-1. When f is close to one, both models predicted that Si isotopic fractionation does not affect the

solution isotopic ratios. In general, experiments with secondary phase precipitation have high Si concentration so *f* is likely very close to one.

Furthermore, in all our experiments, data for all three isotopes were consistently fit with the same albite dissolution rates. There is no observed systematic discrepancy among the isotopes. These data provide strong evidence that isotopic fractionation has little effect on the isotopic ratios of the experimental aqueous solutions.

However, secondary mineral precipitation could occur on the surfaces of the dissolving minerals and block reaction sites. Zhu et al. (2010) found that precipitation of sanidine on the dissolving albite surfaces reduced the albite dissolution rates in the experiments by Alekseyev et al. (1997). Therefore, whether secondary mineral precipitation will interfere with measurements of dissolution rates must be evaluated as a case by case basis.

As shown in Section 4.1, significant Si isotope fractionation was observed during albite dissolution. Using the largest fractionation factor found in this study at pH 3, $^{29}\epsilon_{sol-ab}=-1.49\%$, we calculated Eqs. (32)–(34) that ignoring isotope fractionation would result in ~0.0001 in model prediction of 29 Si for Exp #1-1 at day 270, which is within analytical uncertainty and corresponds to an error in rate of <0.05%

In our experiments, the effects of isotopic fractionation from albite dissolution and secondary phase precipitation on the solution isotopic compositions were opposite, which cancel out their effects on rate determination. As shown before, lighter elements were preferentially released from albite, but also preferentially incorporated into the secondary phase.

4.6. Determination of secondary phase precipitation rates

Combining the solution's isotope ratios with the Si concentration data allows the rate of precipitation of secondary phases to be found using Eq. (10). Fig. 10 shows how this works. For Exp #7-1 silica concentrations ([SiO₂]) calculated from isotope mixing (IX), assuming no secondary mineral precipitation (Model A, red line), are higher than the concentrations calculated from isotope isotope dilution (ID). The solution in this experiment was supersaturated with respect to kaolinite and contained kaolinite seed material. Model B, which takes account of the amount of Si precipitated in a secondary phase with a stoichiometry of Al_2Si_2 reconciles the differences between elemental Si concentrations measured with ID and IX methods.

The [Al] data provided another constraint for the secondary mineral precipitation rates, and the Al:Si stoichiometry in the secondary phase. Although the precipitate was not identified, a precipitate with a stoichiometry of Al_2Si_2 fits both Si and Al concentration data well. In our experiments, the long-term apparent rate ratio r'_{ab}/r'_{kao} is ~2, indicating the combined dissolution–precipitation reactions conserve Al. This constant rate ratios indicates a coupling between dissolution and precipitation reactions (Zhu, 2009; Zhu et al., 2010). Zhu and co-workers advocated that coupled reactions are an important reason for the difference between field and laboratory rates (Zhu, 2005, 2009; Zhu and Lu, 2009; Zhu et al., 2004, 2006, 2010).

For Exp #4-1, where the solution was undersaturated with respect to kaolinite, $[SiO_2]$ calculated from isotope mixing (IX) was always the same as $[SiO_2]$ calculated from isotope isotope dilution (ID). In this case Model A successfully predicted $[SiO_2]$ for Exp #4-1 from both IX and ID methods because no secondary precipitate formed.

5. Discussions

5.1. Comparison with albite dissolution rates in the literature

The overarching question is "does the Si isotope doping method actually work when there is secondary phase precipitating?" For the past three decades, albite dissolution rates have been measured by numerous scientists with various experimental designs (Blum and Stillings,

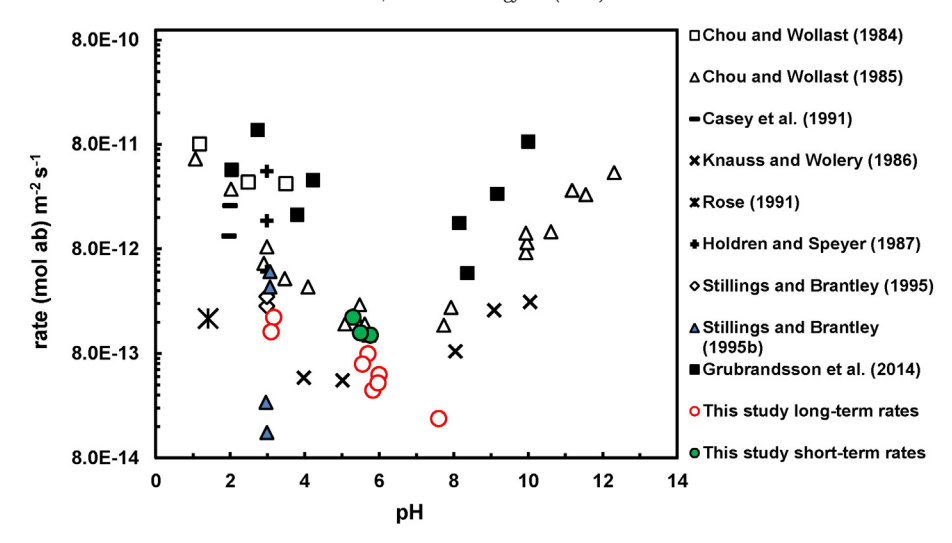


Fig. 13. Comparison of albite dissolution rates from the literature with those from this study plotted pH (at ~25 °C). The solid green circles are from short-term experiments (t < 10 days) and the red open circles are from experiments lasting longer than 10 days. (For interpretation of the references to color in this figure legend, the reader is referred to the web version of this article.)

1995; Gudbrandsson et al., 2014). All previous work was based on the "conventional method", measuring the rate of elemental Si release.

Fig. 13 compares the albite dissolution rates in this study to those of the conventional method over a wide pH range. Significant discrepancies exist among rates measured by different authors. At pH ~5, our far from equilibrium (Exp #4-1) "short-term rates" of ~1.20 \times 10 $^{-12}$ mol m $^{-2}$ s $^{-1}$ (3–10 days) are consistent with rates ~1.25 \times 10 $^{-12}$ mol m $^{-2}$ s $^{-1}$ from Chou and Wollast (1985). Our far from equilibrium "long-term rates" of 6.5 \times 10 $^{-13}$ mol m $^{-2}$ s $^{-1}$ (10–60 days) are twice as slow as those from Chou and Wollast (1985), but are consistent with those from Knauss and Wolery (1986).

At pH 7.6, our rate is more than one order of magnitude slower than those from Knauss and Wolery (1986) and Chou and Wollast (1985). Gudbrandsson et al. (2014) did not measure albite dissolution rates in this pH range. At pH 3, a wide range of albite dissolution rates spanning three orders of magnitude is found in the literature. Our rate is one order of magnitude slower than those from Chou and Wollast (1985) and two orders of magnitude slower than those of Oelkers and co-workers (Gudbrandsson et al., 2014).

Numerous explanations have been proposed for the inter-laboratory discrepancies in measured albite rates, including duration, composition, degree of Al–Si–O order (Zhang and Lüttge, 2009; Fischer et al., 2012), grain size (Fischer et al., 2012), and sample preparation. Notably, differences in sample preparation could result in discrepancies in rates of up to two orders of magnitude (Beig and Lüttge, 2006).

Our experiments, however, were distinguished from previous studies because of our longer experimental durations. All our experiments extended to \sim 30 days. Some lasted to 60 days, 127 days, and 270 days. The duration of albite dissolution experiments by Gudbrandsson et al. (2014) lasted for \sim 3 days or \sim 10 days, by Knauss and Wolery (1986) for 25 days, and by Chou and Wollast (1985) for \sim 10 days. In our experiments, we observed that rates stabilize after 3–4 days (Fig. 7) for most of our experiments.

Long-term rates are difficult to measure with conventional methods. Knauss and Wolery (1986) reported a "loss of signal" after 25 days for albite dissolution at 25 °C and pH 5. See Fig. 7b. They regarded their rate values as the upper limit. In our experiments, we detected reactions after 270 days. The analytical uncertainty for Si isotope fractions is ± 0.0005 . In contrast, the Mo-blue method measures the elemental Si concentrations with an uncertainty of $\pm 4\%$ (Gruber et al., 2013) and the ICP-OES method $\pm 10\%$ (Gudbrandsson et al., 2014). For our pH 3 experiments, ²⁸Si measured at day 177 is 0.34605 and at day 270 is 0.4099. The difference (0.06385) exceeds the analytical uncertainties

by two orders of magnitude. For our experiment at pH 5, from day 30 to day 60, 28 Si changed from 0.1343 to 0.1806. Therefore, we were able to measure what Knauss and Wolery (1986) could not using Si concentrations based on chemical analysis. At pH 7.6, the reaction is very slow. From day 84 to day 128, 28 Si changed from 0.0708 to 0.0919. In contrast, Knauss and Wolery (1986) stopped the experiments at day 10 because the analytical uncertainties exceeded the detection in [SiO₂] differences. They were only able to provide an upper limit value.

However, while the isotope doping method has greatly improved the precision and sensitivity of the rate measurements, the accuracy of rate determination is still subject to the vagaries of unknown or uncontrolled variables. Exp #4-1, 5-1, 6-1, and 7-1 were all conducted at pH ~5.5. The long-term, "far from equilibrium" rates range from 3.55×10^{-13} to 7.94×10^{-13} mol m⁻² s⁻¹. As mentioned above, measured rates in replicate experiments can vary significantly.

5.2. Rates as a function of saturation

The Si isotope doping method can also measure dissolution rates at near equilibrium conditions because neither the precipitation of a Sicontaining secondary phase nor the Si isotope fractionation during the secondary precipitation have measurable effects on the rate determination. Some previous studies observed 5 to 50 times of slower Si release rates in the $-35 < \Delta G_{\rm r} < 0$ kJ/mol near equilibrium region. These slower rates might have been caused by secondary phase precipitation (see detailed discussions in Burch et al., 1993; Hellmann and Tisserand, 2006) because several secondary phases were supersaturated. Careful electron microscopy did not positively identify secondary phases. The Si isotope doping method can resolve this problem.

In Fig. 8, two Burch type $r-\Delta G_r$ curves were drawn with parameters from Burch et al. (1993) and Hellmann and Tisserand (2006) and a far from equilibrium albite dissolution rate of 6.53×10^{-13} mol m $^{-2}$ s $^{-1}$. A transition state theory rate law curve is also shown. The experimental data points represent long-term rates at pH ~5.5 corresponding to ΔG_r from -62 to -25 kJ/mol. The experiments started with different 29 Si concentrations, but they were not close enough to equilibrium. Future experiments can start with solutions with higher 29 Si concentrations. Table 5 shows the predicted albite dissolution rates according to these three rate laws at ΔG_r of -5, -10, -15, and -20 kJ/mol. These rates are significantly different from each other so that we could measure r_{ab} to test these rate laws. Fig. 14a shows that the possible experimental design in terms of initial [SiO₂] in the doped solutions, solid:water ratios, and

Table 5 Predicted albite dissolution rates according to Burch et al. (1993); Hellmann and Tisserand (2006) and transition state theory rate laws at ΔG_r of -5, -10, -15, and -20 k//mol.

$\Delta G_{\rm r}$ (kJ/mol)	Predicted albite dis	Predicted albite dissolution rates (mol ab $\mathrm{m}^{-2}\mathrm{s}^{-1}$)								
	Burch rate law	Hellmann and Tisserand rate law	Transition state theory rate law							
-5	4.76×10^{-14}	1.06×10^{-14}	5.68×10^{-13}							
-10	5.69×10^{-14}	2.22×10^{-14}	6.42×10^{-13}							
-15	5.83×10^{-14}	6.11×10^{-14}	6.52×10^{-13}							
-20	6.08×10^{-14}	1.49×10^{-13}	6.53×10^{-13}							

initial $^{29}Si/^{28}Si$ ratio. Fig. 14b shows the predicted xSi versus *t* and there are measurable $^{29}Si/^{28}Si$ changes even after 60 days of reaction.

However, very close to equilibrium, the backward reaction will be significant, and that affects the isotope ratios. Liu et al. (2016) used the isotope doping method and measured dissolution and precipitation rates at equilibrium. As reactions proceeded, ²⁹Si was deposited on quartz surface and the quartz surface had a Si isotopic composition different from the bulk quartz, rendering the isotope doping method inoperable. Either the experimental design or interpretation models need to be modified or improved before measuring rates very close to equilibrium is possible.

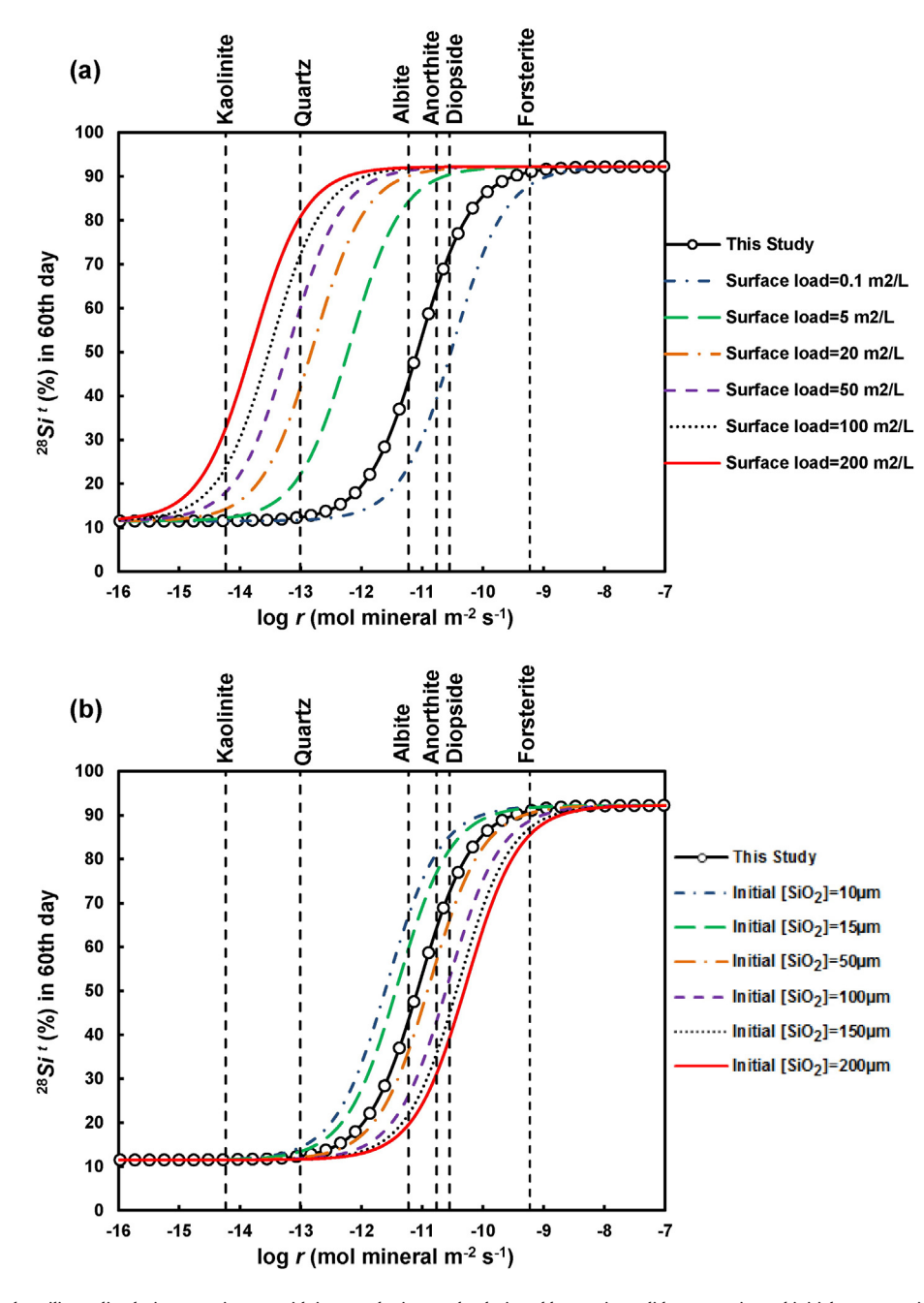


Fig. 14. Graphic illustration that silicate dissolution experiments with isotope doping can be designed by varying solid:water ratio, and initial concentration of doped ²⁹Si solutions. The curves show predicted ²⁸Si fractions of experimental solution at day 60, using the basic information from Exp #7-1, by varying (a) surface area load (mineral:water ratios and grain sizes), and (b) initial [²⁹SiO₂]. Mineral dissolution rates are from Brantley (2008) at pH 3. Burch et al. (1993) Free energy dependence of albite dissolution kinetics at 80 °C and pH 8.8. *Chemical Geology* 105, 137–162. Hellmann and Tisserand (2006) Dissolution kinetics as a function of the Gibbs free energy of reaction: an experimental study based on albite feldspar. *Geochim. Cosmochim. Acta* 70, 364–383. Knauss and Wolery (1986) Dependence of albite kinetics on pH and time at 25 °C and 70 °C. *Geochimica et Cosmochimica Acta* 50, 2481–2497.

5.3. Measurement of reaction rates for other silicate minerals and glasses

Results in this study also demonstrate that we now can measure reaction rates for silicates with a wide range of dissolution rate values. Silicate mineral dissolution rates vary ~4 orders of magnitude (Brantley, 2008). We can vary the initial $^{29}Si/^{28}Si$, $[SiO_2]^{f0}$, and solid:water ratio in the reactor (or surface area load) to find the optimal conditions for measuring individual silicate mineral. Fig. 14 shows the simulations that used the conditions of Exp #7-1 as the starting point and predicted the values of $^{28}Si^t$ at day 60. The curves show the relationship between $^{28}Si^t$ at day 60 and dissolution rates. Each curve represents a particular surface area load (m^2/L). The steeper the curve, the tighter constraints from the Si isotope fraction data.

Fig. 14a shows that the predicted 28Si fraction after 60 days change dramatically. Fig. 14b shows the effects of different initial [SiO₂]. Varying the $^{29}Si/^{28}Si$ in the doping solution would not increase the sensitivity much (not shown). For kaolinite with a dissolution rate of $8.7\times10^{-15}\,\mathrm{mol}\;\mathrm{m}^{-2}\,\mathrm{s}^{-1}$ at 25 °C and pH 4 (Brantley, 2008) with a specific surface area of 11.8 m^2/g , conditions of initial solution 10–100 $\mu\mathrm{M}$ SiO_{2,aq}, solid:water ratio of 2–10 g/L would give highly sensitive measurements of rates. Comparing quartz with forsterite dissolution, we would need lower initial [SiO₂] and high surface area load for quartz and high initial [SiO₂] and low surface area load for forsterite. By varying these conditions, the full range of silicate mineral dissolution rates can be measured at ambient conditions.

6. Conclusions and remarks

Here we present new experimental data and quantitative modeling results to demonstrate that the Si isotope doping method works well for determining silicate dissolution rates while a Si-containing secondary phase is precipitating. In ²⁹Si-doped albite dissolution batch experiments, experimental solution ²⁹Si and ²⁸Si versus time curves uniquely determined the albite dissolution rates with high precision. These curves were not significantly affected by Si isotopic fractionation during albite dissolution, the precipitation of a Sicontaining secondary phase, or the Si isotopic fractionation during secondary phase precipitation. Combining isotope data with Si concentrations determined from the Si isotope dilution method also gave precipitation rates. Therefore, this method is superior to experiments that measure the release rates using solution analysis. The isotope doping method is suitable for measuring silicate reaction rates at ambient temperatures, circumneutral pH, and in the presence of simultaneous dissolution and precipitation reactions. However, although the precision and sensitivity has greatly improved over conventional solution chemistry based methods, the accuracy of the rate determination, in terms of variation from experiment to experiment, have a similar pattern to that in literature.

Experimental data and quantitative analysis also demonstrated the potential of this method for experimental designs that have not yet been fully explored. Dissolution of a small amount of albite can be detected using Si isotope doping with analytical uncertainties of ± 0.0005 –0.001. The albite dissolution rates show dependence on the saturation of albite. The rate $-\Delta G_r$ relationships are controversial in the geochemistry community (Oelkers, 2001; Hellmann and Tisserand, 2006; Arvidson and Luttge, 2010), with regard to "Burch-type rate law" versus transition state rate laws. Therefore, the isotope doping method has the potential to measure silicate dissolution rates at various saturation states and determine the rate $-\Delta G_r$ relationships. However, experiments very close equilibrium when backward reaction is significant will have ²⁹Si deposited on the mineral surface and re-dissolved into the solution. This will complicate the interpretation and more innovative experimental design is necessary.

Acknowledgments

CZ acknowledges U.S. NSF grant EAR-1225733. Although the work was partly sponsored by an agency of the United States Government, the views and opinions of authors expressed herein do not necessarily state or reflect those of the United States Government or any agency thereof. ZY Liu was supported by a grant from Zhejiang University. HL Yuan acknowledges funding from the State Key Laboratory of Continental Dynamics for Si isotope analysis.

References

- Alekseyev, V.A., Medvedeva, L.S., Prisyagina, N.I., Meshalkin, S.S., Balabin, A.I., 1997. Change in the dissolution rates of alkali feldspars as a result of secondary mineral precipitation and approach to equilibrium. Geochim. Cosmochim. Acta 61, 1125–1142.
- Arvidson, R.S., Luttge, A., 2010. Mineral dissolution kinetics as a function of distance from equilibrium — new experimental results. Chem. Geol. 269 (1–2), 79–88.
- Beck, J.W., Berndt, M.E., Seyfried Jr., W.E., 1992. Application of isotopic doping techniques to evaluation of reaction kinetics and fluid/mineral distribution coefficients: an experimental study of calcite at elevated temperatures and pressures. Chem. Geol. 97 (1–2) 125–144
- Beig, M.S., Lüttge, A., 2006. Albite dissolution kinetics as a function of distance from equilibrium: implications for natural feldspar weathering. Geochim. Cosmochim. Acta 70 (6), 1402–1420.
- Berndt, M.E., Seyfried, W.E., 1999. Rates of aragonite conversion to calcite in dilute aqueous fluids at 50 to 100 °C: experimental calibration using Ca-isotope attenuation. Geochim. Cosmochim. Acta 63 (3–4), 373–381.
- Berner, R.A., Berner, E.K., 1997. Silicate weathering and climate. In: Ruddiman, W.F. (Ed.), Tectonic Uplift and Climate Change. Plenum Press, pp. 353–364.
- Blum, A.E., Stillings, L.L., 1995. Feldspar dissolution kinetics. In: Brantley, S.L. (Ed.), White, A.F.Chemical Weathering Rates of Silicate Minerals. Reviews in Mineralogy, Mineralogical Society of America, pp. 291–346
- Brantley, S.L., 1992. Kinetics of dissolution and precipitation-experimental and field results. Proceedings of the Seventh International Conference on Water–Rock Interactions, 7, Park City, Utah: Rotterdam, Balkema, pp. 465–469.
- Brantley, S.L., 2008. Kinetics of mineral dissolution. In: Brantley, S.L., Kubicki, J.D., White, A.F. (Eds.), Kinetics of Water–Rock Interaction. Springer, New York, pp. 151–210.
- Braunauer, S., Emmett, P.H., Teller, E., 1938. Adsorption of gases in multimolecular layers. J. Am. Chem. Soc. 60, 309–319.
- Burch, T.E., Nagy, K.L., Lasaga, A.C., 1993. Free energy dependence of albite dissolution kinetics at 80 °C and pH 8.8. Chem. Geol. 105 (1–3), 137–162.
- Chou, L., Wollast, R., 1985. Steady-state kinetics and dissolution mechanisms of albite. Am. J. Sci. 285, 963–993.
- Drever, J.I., Clow, D.W., 1995. Weathering rates in catchments. In: White, A.F., Brantley, S.L. (Eds.), Chemical Weathering Rates of Silicate Minerals. Reviews in Mineralogy. Mineralogical Society of America, pp. 463–481.
- Federer, C.A., et al., 1989. Long-term depletion of calcium and other nutrients in eastern US forests. Environ. Manag. 13, 593–601.
- Fischer, C., Arvidson, R.S., Lüttge, A., 2012. How predictable are dissolution rates of crystalline material? Geochim. Cosmochim. Acta 98, 177–185.
- Gaillardet, J., 2008. Isotope geochemistry as a tool for deciphering kinetics of water-rock interaction. In: Brantley, S.L., Kubicki, J.D., White, A.F. (Eds.), Kinetics of Water-Rock Interaction. Springer, New York.
- Georg, R.B., Reynolds, B.C., Frank, M., Halliday, A.N., 2006. New sample preparation techniques for the precise determination of the Si isotope composition of natural samples using MC-ICP-MS. Chem. Geol. 235, 95–104.
- Georg, R.B., Zhu, C., Reynolds, B.C., Halliday, A.N., 2009. Stable silicon isotopes of ground-water, feldspars, and clay coatings in the Navajo Sandstone aquifer, Black Mesa, Arizona, USA. Geochim. Cosmochim. Acta 73 (8), 2229–2241.
- Govett, G., 1961. Critical factors in the colorimetric determination of silica. Anal. Chim. Acta 25 (1), 69–80.
- Gruber, C., Harpaz, L., Zhu, C., Bullen, T.D., Ganor, J., 2013. A new approach for measuring dissolution rates of silicate minerals by using silicon isotopes. Geochim. Cosmochim. Acta 104 (0), 261–280.
- Gruber, C., Zhu, C., Georg, R.B., Zakon, Y., Ganor, J., 2014. Resolving the gap between laboratory and field rates of feldspar weathering. Geochim. Cosmochim. Acta 147, 90–106
- Gudbrandsson, S., Wolff-Boenisch, D., Gislason, S.R., Oelkers, E.H., 2014. Experimental determination of plagioclase dissolution rates as a function of its composition and pH at 22 °C. Geochim. Cosmochim. Acta 139 (0), 154–172.
- Harlow, G.E., Brown, G.E., 1980. Low albite: an X-ray and neutron diffraction study. Am. Mineral. 65, 986–995.
- Harouiya, N., Oelkers, E.H., 2004. An experimental study of the effect of aqueous fluoride on quartz and alkali-feldspar dissolution rates. Chem. Geol. 205, 155–167.
- Helgeson, H.C., Delany, J.M., Nesbitt, H.W., Bird, D.K., 1978. Summary and critique of the thermodynamic properties of rock forming minerals. Am. J. Sci. 278A, 569–592.
- Hellmann, R., Tisserand, D., 2006. Dissolution kinetics as a function of the Gibbs free energy of reaction: an experimental study based on albite feldspar. Geochim. Cosmochim. Acta 70, 364–383.
- Holdren, G.R., Berner, R.A., 1979. Mechanism of feldspar weathering. I. Experimental studies. Geochim. Cosmochim. Acta 43, 1161–1171.
- Knauss, K.G., Wolery, T.J., 1986. Dependence of albite kinetics on pH and time at 25 °C and 70 °C. Geochim. Cosmochim. Acta 50, 2481–2497.

- Lasaga, A.C., Soler, J.M., Ganor, J., Burch, T.E., Nagy, K.L., 1994. Chemical weathering rate laws and global geochemical cycles. Geochim. Cosmochim. Acta 58 (10), 2361–2386.
- taws and grobal geochemical cycles. Geochini. Cosmochini. Acta 58 (10), 2361–2386. Likens, G.E., et al., 1998. The biogeochemistry of calcium at Hubbard Brook. Biogeochemistry 41, 89–173
- Liu, Z., Zhang, Y.L., Yuan, H.L., Rimstidt, J.D., C. Z., 2016. A stable isotope doping method to test the range of applicability of detailed balance. Geochem. Perspect. Lett. 2 (1), 78–86.
- Lu, P., et al., 2013. Coupled alkali feldspar dissolution and secondary mineral precipitation in batch systems: 2. New experiments with supercritical CO₂ and implications for carbon sequestration. Appl. Geochem. 30, 75–90.
- Oelkers, E.H., 2001. General kinetic description of multioxide silicate mineral and glass dissolution. Geochim. Cosmochim. Acta 65 (21), 3703–3719.
- Opfergelt, S., Delmelle, P., 2012. Silicon isotopes and continental weathering processes: assessing controls on Si transfer to the ocean. Compt. Rendus Geosci. 344 (11–12), 723–738
- Parkhurst, D.L., Appelo, C.A.J., 1999. PHREEQC 2.15 A computer program for speciation, batch-reaction, one-dimensional transport and inverse geochemical calculation. Water-Resources Investigation Report 99-4259. U.S. Geological Survey.
- Seimbille, F., Zuddas, P., Michard, G., 1998. Granite–hydrothermal interaction: a simultaneous estimation of the mineral dissolution rate based on the isotopic doping technique. Earth Planet. Sci. Lett. 157 (3–4), 183–191.
- Smith, J.V., Brown, W.L., 1988. Feldspar Minerals. second ed. Springer Verlag, Berlin 1. 1, 828 pp. (828 pp.).
- Spycher, N.F., Sonnenthal, E.L., Apps, J.A., 2003. Fluid flow and reactive transport around potential nuclear waste emplacement tunnels at Yucca Mountain, Nevada. J. Contam. Hydrol. 62–63, 653–673.
- Velbel, M.A., 1990. Influence of temperature and mineral surface characteristics on feldspar weathering rates in natural and artificial systems: a first approximation. Water Resour. Res. 26, 3049–3053.
- White, C., Strasizar, B.R., Granite, E.J., Hoffman, J.S., Pennline, H.W., 2003. Separation and capture of CO₂ from large stationary sources and sequestration in geological formations coalbeds and deep saline aquifers. J. Air Waste Manag. Assoc. 53,

- Yang, L., Steefel, C.I., 2008. Kaolinite dissolution and precipitation kinetics at 22 °C and pH 4. Geochim. Cosmochim. Acta 72 (1), 99–116.
- Zhang, L., Lüttge, A., 2009. Theoretical approach to evaluating plagioclase dissolution mechanisms. Geochim. Cosmochim. Acta 73 (10), 2832–2849.
- Zhu, C., 2005. In situ feldspar dissolution rates in an aquifer. Geochim. Cosmochim. Acta 69 (6), 1435–1453.
- Zhu, C., 2009. Geochemical modeling of reaction paths and geochemical reaction networks. In: Oelkers, E.H., Schott, J. (Eds.), Thermodynamics and Kinetics of Water–Rock Interaction. Reviews in Mineralogy. Mineralogical Society of America, pp. 533–569.
- Zhu, C., Lu, P., 2009. Alkali feldspar dissolution and secondary mineral precipitation in batch systems: 3. Saturation states of product minerals and reaction paths. Geochim. Cosmochim. Acta 73 (11), 3171–3200.
- Zhu, C., Blum, A.E., Veblen, D.R., 2004. Feldspar dissolution rates and clay precipitation in the Navajo aquifer at Black Mesa, Arizona, USA. In: Wanty, R.B., Seal, R.R.I. (Eds.), Water–Rock Interaction. A.A. Balkema, Saratoga Springs, New York, pp. 895–899.
- Zhu, C., Lu, P., Zheng, Z., Ganor, J., 2010. Coupled alkali feldspar dissolution and secondary mineral precipitation in batch systems: 4. Numerical modeling of kinetic reaction paths. Geochim. Cosmochim. Acta 74 (14), 3963–3983.
- Zhu, C., Veblen, D.R., Blum, A.E., Chipera, S.J., 2006. Naturally weathered feldspar surfaces in the Navajo Sandstone aquifer, Black Mesa, Arizona: electron microscopic characterization. Geochim. Cosmochim. Acta 70 (18), 4600–4616.
- Zhu, C., et al., 2014. Silicon isotopes as a new method of measuring silicate mineral reaction rates at ambient temperature. Procedia Eath Planet. Sci. 10, 189–193.
- Ziegler, K., Chadwick, O.A., Brzezinski, M.A., Kelly, E.F., 2005. Natural variations of delta Si-30 ratios during progressive basalt weathering, Hawaiian Islands. Geochim. Cosmochim. Acta 69 (19), 4597–4610.
- Zuddas, P., Seimbille, F., Michard, G., 1995. Granite–fluid interaction at near-equilibrium conditions: experimental and theoretical constraints from Sr contents and isotopic ratios. Chem. Geol. 121 (1–4), 145–154.